Bernd Taschler

Strongly correlated systems under the influence of an electric field: A cluster perturbation approach

MASTER THESIS

For obtaining the academic degree
Diplom-Ingenieur

Master Program of
Technical Physics

Graz University of Technology

Supervisor:
Univ.-Prof. Dr.rer.nat. Enrico Arrigoni
Institute of Theoretical and Computational Physics

Graz, May 2011

Though this be madness, yet there is a method in't.

Hamlet [Act II, Scene II]

Abstract

Strongly correlated systems are especially important for understanding the properties of nano-scale structures and exotic materials such as high-temperature superconductors. As experimental techniques steadily improve and potential applications are being envisioned, the need for a theoretical explanation of correlation-induced phenomena is all the more fortified.
Within a wide range of theoretical approaches, in the area of many-body physics the Hubbard model has been captivating most attention. In this thesis we treat the fermionic Hubbard model in the framework of Cluster Perturbation Theory (CPT) and develop a pseudoparticle description of single-particle excitations. A static or periodic external electric field is applied which as a consequence drives the system out of equilibrium and gives rise to a particle current.
A variety of physical phenomena emerge, such as damping of Bloch oscillations, metal-to-insulator transitions and Mott insulating phases. We look at the characteristics of a Mott insulator and compare them with the features of conventional band insulators. Furthermore, we investigate the time evolution of the current density and the reciprocity of kinetic and potential energies depending on the strength of electron-electron interactions.
Apart from half-filled systems in one and two spatial dimensions we are also concerned with band doping and its effect on the system's response to an external field.

Kurzfassung

Stark korrelierte Systeme sind insbesondere für das Verständnis der Eigenschaften von Nanostrukturen und exotischer Materialien, wie zum Beispiel Hochtemperatur-Supraleiter, von großer Bedeutung. Nicht zuletzt im Hinblick auf die ständige Verbesserung der verfügbaren experimentellen Methoden sowie potentielle Anwendungen ist es notwendig ein theoretisches Fundament für die Beschreibung von korrelationsbedingten Phänomenen zu etablieren.
Auf dem weiten Gebiet der theoretischen Modellierung atomarer Systeme hat vor allem im Bereich der Vielteilchenphysik das Hubbard Modell das größte Interesse auf sich gezogen. In dieser Arbeit formulieren wir im Rahmen der Cluster Störungstheorie einen Pseudoteilchen-Ansatz für das Fermi-Hubbard Modell. Ein statisches oder oszillierendes äußeres elektrisches Feld treibt das System aus dem Gleichgewicht und erzeugt einen elektrischen Strom.
Es können verschiedene physikalische Effekte beobachtet werden, wie korrelationsabhängig gedämpfte Bloch Oszillationen, Metall-Isolator Übergänge und Mott-isolierende Phasengebiete. Wir behandeln die Besonderheiten von Mott-Isolatoren und vergleichen diese mit den Eigenschaften von gewöhnlichen Bandisolatoren. Darüber hinaus, werden die Zeitentwicklung der Stromdichte sowie das Wechselspiel zwischen kinetischer und potentieller Energie in Abhängigkeit von der Elektron-Elektron Wechselwirkung untersucht.
Neben halb gefüllten Anordnungen in ein und zwei Raumdimensionen, betrachten wir außerdem die Auswirkungen von Band-Dotierungen auf das Strom-Zeit Verhalten des Systems unter dem Einfluss des externen elektrischen Feldes.

Contents

Chapter 1

Introduction

Strongly correlated systems at the center of interest in many areas of condensed matter or many-body physics. Their intriguing properties which give rise to complex and at times exotic physical phenomena call on the attention of theorists and experimentalists alike.
The processes that govern the formation of high-temperature superconductors, for example, which were discovered in the late 1980s [1], are still not very well understood. Especially cuprate compounds (see Fig. 1.1 for an example), manganites or the family of low-dimensional vanadates [2] and other advanced materials, such as organic conductors and colossal-magnetoresistance materials, belong to the category of strongly correlated systems and have been the focus of extensive research in recent years.
In contrast to materials where correlations between particles play a minor role, the theoretical description of strong interaction constitutes a serious challenge because the resulting phenomena cannot be inferred from the behavior of individual particles alone.

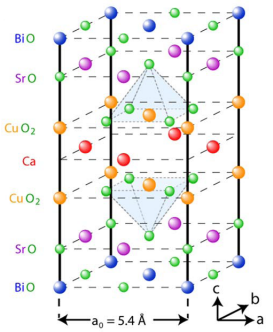

Figure 1.1: Atomic structure of BSCCO as an example for a high-temperature superconductor belonging to the family of cuprates. Shown is the top half of the $Bi_2Sr_2CaCu_2O_8$ unit cell (the lower half is identical except for a translation by $a_0/2$ along the a axis). Crystal axes a, b, and c are indicated [3]. As for most high-temperature superconductors, the superconductivity is a mainly two-dimensional effect that emanates from the copper-oxide planes.

In a strongly interacting system the motion of each single particle is influenced by the position and momentum of, at least in principle, all other particles. Most importantly for the particles' correlations are long-range Coulomb forces.
In many cases, only the short range part of the interaction produces genuine correlation effects, since long-range contributions can be effectively screened. One of the most influential models is

the Hubbard model, which was proposed already half a century ago. Despite much effort a general solution is still not tangible and only in the one-dimensional case a solution is available.
The Hubbard model and its variants play a decisive role in a large part of theoretical condensed matter physics. The model is particularly useful and widespread in the context of strongly correlated electron systems such as narrow band materials and transition metal oxides [4].
In spite of its simple definition, the Hubbard model is believed to exhibit various interesting phenomena including metal-insulator transitions, antiferromagnetism, ferrimagnetism, ferromagnetism, Tomonaga-Luttinger liquid, and superconductivity [5].

The tight-binding Hubbard model accounts for the particle motion through an atomic lattice by means of 'hopping' processes and includes non-linear repulsive Coulomb interactions that act only locally, i.e. the occupation of the same atomic site by two particles is punished with an energy fine. Although the model appears rather simple at the outset, the interplay of kinetic and interacting parts of the Hamiltonian prove difficult to reconcile mathematically.
The necessity of additional simplifications leads to a variety of numerical methods that have become popular in recent decades. Examples of such implementations are Dynamical Mean Field Theory (DMFT), Density Matrix Renormalization Group (DMRG), the Hartree-Fock method and perturbative approaches. The latter consider a breaking up of the whole lattice into smaller clusters which then can be solved exactly.
In this thesis we will adopt a variant of that kind, that is Cluster Perturbation Theory (CPT), and consolidate the corresponding Hamiltonian with a description of an externally applied field. By turning on the electric field at a certain time, the system is driven out of equilibrium provoking non-linear behavior in response.

Experimental realizations of atomic systems that match the characteristics of the Hubbard model have become very sophisticated in recent years. Several groups succeeded to trap a Bose-Einstein condensate in an optical lattice, thereby artificially reproducing a nearly perfect Bose-Hubbard model. Due to the even more severe temperature requirements in the case of ultracold Fermi gases, it is harder to bring about the fermionic Hubbard model. For more details see for example Refs. [6] and [7].

It has been suggested that the effects induced by an electric field and the possibility of tuning the carrier concentration may be used in applications featuring complex materials such as organic conductors, high-temperature superconductors and colossal magnetoresistance compounds [8].
The conductance of nanoelectronic structures, for example, can be administered by tuning the carrier density and applying an electric field. The controllability of electronic properties, with regard to its success in semiconductor devices, has the potential to offer a wide range of new perspectives for applications of strongly correlated materials.

Significant progress in experimentally reproducing nano-scale materials, such as quantum dots, and unusual physical effects like the strong change in the optical transmission in the transition-metal oxide Sr_2CuO_3 and the dielectric breakdown of a Mott insulator that occurs in quasi-onedimensional cuprates such as Sr_2CuO_3 and $SrCuO_2$ [9] require a thorough theoretical understanding of the underlying phenomena that lead to these effects.

The importance of strong electric fields comes apparent when dealing with nanoscale devices where electric potentials in the range of a few volts produce electric fields of order 10^5 to $10^6 V/m$. To understand the response of an interacting system to a formidable electric field, especially non-linear current-voltage characteristics, is therefore crucial for realizing devices that embody correlation effects.

Outline

This thesis presents a numerical analysis of the time evolution of the non-equilibrium current density originating from an externally applied electric field. It is organized as follows: In chapter two we lay out the methodological framework of our method and give a general introduction to the Hubbard model with some emphasis on the one-dimensional case.

Chapter three deals with the formulation of Cluster Perturbation Theory and the corresponding Hamiltonian in terms of a pseudoparticle approach as it has been briefly formulated in Ref. [10]. We then proceed with the incorporation of the electric field and develop a description for the time evolution of the system.
This second part of chapter three together with chapters four and five constitutes basically the original work carried out within this thesis.

In chapter four we concentrate on the theoretical formulation and calculation of expectation values for the time resolved current response and discuss the characteristics of a Mott insulator as well as the origin of Bloch oscillations.

Numerical results are discussed in chapter five with regard to one- and two-dimensional lattices and including various phenomena that arise from applying static or oscillating electric fields, such as Bloch oscillations, metallic as well as Mott insulating behavior, metal-insulator transitions and the possibility of a dielectric breakdown of the Mott insulator. In addition to half-filled lattices, we are investigating the effects of doping on the system's response to the external field.

Finally, chapter six provides some concluding remarks and a brief outlook for potential further research.

Chapter 2

Formalism

In condensed matter physics when we are looking at complex electronic and atomic systems, one maps the real system onto idealized and simplified models and hopes that these models are able to describe as many properties of the original system as accurately as possible. This mathematical mapping results in a certain Hamiltonian which contains the main features of the underlying model.

Effective single particle treatments do not include correlation effects between two distinct particles but can only account for (averaged or screened) interactions between one particle and a 'particle-sea' containing the rest. Especially when Coulomb correlations play an important role, these single particle models fail and two-particle interactions have to be incorporated into the Hamiltonian.
However, when we try to take those particle-particle interactions into account, we immediately face the obstacle that a typical solid consists of some 10^{23} particles which, in principle, all interact with one another. Since any n-body problem (with $n > 2$) can only be solved by means of approximations, it is clear that one has to resort to some sort of model that helps to simplify matters significantly in one way or the other.

There are several models at hand, each of them stressing certain features of the underlying physics while approximating other features (or sometimes neglecting them altogether). In the case of strong electron-electron correlations the most prominent model since its introduction in the early sixties of the 20^{th} century is the Hubbard model.
Although it may strike one as rather simple, the interplay of kinetic and potential energy needs quite a bit of effort to reconcile. A major problem is given by the fact that the kinetic part of the Hamiltonian is diagonal in momentum space whereas the interaction part is diagonal in real space.

In this chapter, after some introductory and rather general quantum mechanical remarks in Sec. 2.1, we will concentrate on general properties of the widely popular Hubbard model (Sec. 2.2) as well as on the closely related Falicov-Kimball model (Sec. 2.3).

2.1 Second quantization and Wannier functions

In the following section we will apply the occupation number formalism to quantum mechanics which is commonly referred to as 'second quantization'. For a more rigorous and thorough treatment see for example Refs. [11, 12, 13, 14].

The general Hamilton operator for a many-body system of electrons and atomic nuclei has the form

$$\begin{aligned}\hat{H} \;=\; &-\; \frac{\hbar^2}{2m_e}\sum_i \nabla_i^2 \;-\; \sum_i\sum_I \frac{Z_I e^2}{|\mathbf{r}_i - \mathbf{R}_I|} \;+\; \frac{1}{2}\sum_{i\neq j}\frac{e^2}{|\mathbf{r}_i - \mathbf{r}_j|} \;- \\ &-\; \frac{\hbar^2}{2M_I}\sum_I \nabla_I^2 \;+\; \frac{1}{2}\sum_{I\neq J}\frac{Z_i Z_J e^2}{|\mathbf{R}_I - \mathbf{R}_J|}\end{aligned} \tag{2.1}$$

where small (capital) letters denote quantities belonging to electrons (ions), Z is the number of protons in the nucleus, e stands for the elementary charge and $\mathbf{r_i}$ ($\mathbf{R}_I$) are position vectors in real space.
Terms 1 and 4 in (2.1) constitute the kinetic energies of electrons and ions. The other three terms describe the potential energy arising from Coulomb interactions between electrons and nuclei, between two electrons and between two atomic nuclei respectively.

Due to the fact that the mass of an atomic nucleus is much larger than the mass of an electron, the movement of the nuclei can be neglected. This means one can set the fourth term to zero as a first approximation (Born-Oppenheimer approx.) and neglect the contribution of the last term to the energy, which would amount to a constant.

Although the Born-Oppenheimer approximation considerably simplifies matters, we would still have to face an infinitely large (and unsolvable) problem if we were to consider all possible interactions between the particles.

For strictly noninteracting electrons the Hamiltonian would have the form

$$\hat{H} \;=\; -\;\frac{\hbar^2}{2m_e}\sum_i \left[\nabla_i^2 \;-\; \mathcal{V}(\mathbf{r}_i)\right] \tag{2.2}$$

where $\mathcal{V}(\mathbf{r}_i) = \sum_I \frac{Z_I e^2}{|\mathbf{r}_i - \mathbf{R}_I|}$ denotes the lattice potential created by the atomic nuclei.

According to Bloch's theorem [15, 16] the eigenfunctions of a periodic lattice are plane waves modulated by the periodicity of the lattice potential $\mathcal{V}(r)$, which gives for any lattice vector $\mathbf{R}$

$$\psi_{\mathbf{k}\alpha}(\mathbf{r}) = e^{\mathrm{i}\,\mathbf{kR}} u_{\mathbf{k}\alpha}(\mathbf{r}) \tag{2.3}$$

where $u_{\mathbf{k}\alpha}(\mathbf{r})$ has the same periodicity as $\mathcal{V}(r)$. $\mathbf{k}$ symbolizes the crystal momentum which takes values inside the Brillouin zone, that is $k \in [-\pi, \pi)$ if the lattice spacing equal is equal to one, and α is the band index.

We assume that we are dealing with atomic orbitals that are localized at the lattice sites, which means that the spacing between atoms is large in comparison to the size of the orbitals. This is called the Tight-Binding model and owing to this approximation we can use a set of states for our basis that corresponds to the atomic orbitals of an isolated ion.
Instead of using plain waves it is convenient to work with Wannier functions as an appropriate basis set in real space

$$w_{\alpha\sigma}(\mathbf{r} - \mathbf{R}_i) = \frac{1}{\sqrt{\Lambda}} \sum_{\mathbf{k}}^{1.BZ} e^{-\,\mathrm{i}\,\mathbf{kR}_i} \psi_{\mathbf{k}\alpha\sigma}(\mathbf{r}) \tag{2.4}$$

Λ is the number of lattice sites, α indicates the orbital and $\mathbf{R}_i$ is the position vector of the i-th atomic site where the orbital is localized.

Wannier functions are essentially wave packets composed of Fourier-transformed Bloch orbitals. This concentrates the wave function of a particle in a small region of space, i.e. a particular site of the lattice. We assume that the bands are well separated and we are interested in the lowest band only.
The amplitudes of the wave functions decrease rapidly over distance, so that the overlap of Wannier functions separated by the lattice spacing is already negligible. The electronic energy bands are very narrow due to the electron's large probability to be found at a particular atomic site. Wannier functions are thus well qualified to describe for example d- or f-orbitals of transition metal oxides where the atomic overlap is comparatively small.
Furthermore, Wannier orbitals localized at different sites i, j as well as belonging to different bands α, β are orthogonal and form a complete basis set:

$$\int d^3r \; w^*_{\alpha\sigma}(\mathbf{r}-\mathbf{R}_i) w_{\beta\sigma'}(\mathbf{r}-\mathbf{R}_j) \;=\; \delta_{\sigma\sigma'}\delta_{\alpha\beta}\delta_{ij} \tag{2.5}$$

$$\sum_{\mathbf{r},\mathbf{r}'}\sum_{i} w^*_{\alpha\sigma}(\mathbf{r}-\mathbf{R}_i) w_{\alpha\sigma}(\mathbf{r}'-\mathbf{R}_i) \;=\; \delta(\mathbf{r}-\mathbf{r}') \tag{2.6}$$

Considering valence bands only with binding energies up to about $10eV$ and one orbital per atom, the annihilation operator for the one-band wave function $\psi_\sigma(\mathbf{r})$ which is located at $\mathbf{R}_i$ can be written in the form

$$\psi_\sigma(\mathbf{r}) \;=\; \frac{1}{\sqrt{\Lambda}} \sum_i c_\sigma(\mathbf{R}_i) w_\sigma(\mathbf{r}-\mathbf{R}_i) \tag{2.7}$$

We write the dependence on $\mathbf{R}_i$ in indexed form and directly obtain the canonical anti-commutation relations and therefore the right operator algebra

$$\begin{aligned} \left\{c_{i\sigma}, c^\dagger_{j\sigma'}\right\} \;\equiv\; c_{i\sigma}c^\dagger_{j\sigma'} + c^\dagger_{j\sigma'}c_{i\sigma} \;&= \delta_{ij}\delta_{\sigma\sigma'} \\ \left\{c_{i\sigma}, c_{j\sigma'}\right\} \;=\; \left\{c^\dagger_{i\sigma}, c^\dagger_{j\sigma'}\right\} \;&= 0 \end{aligned} \tag{2.8}$$

Physically the fermionic creation (annihilation) operators $c^\dagger_{i\sigma}$ ($c_{i\sigma}$) create (annihilate) an electron with spin σ at the i-th lattice site.
And the number operator is defined as

$$\hat{N} \;=\; \sum_{i,\sigma} n_{i\sigma} \;\equiv\; \sum_{i,\sigma} c^\dagger_{i\sigma} c_{i\sigma} \tag{2.9}$$

with eigenvalues 0 and 1, commensurate with empty or occupied sites respectively.

2.2 The Hubbard model

On a historic note, the Hubbard model was proposed individually by Hubbard [17], Gutzwiller [18], who studied d-electrons in ferromagnets, and Kanamori [19] in the seemingly very productive year of 1963. Half a century later, despite extensive research, little progress has been made with regard to fully understanding the model's rich properties. Although the Hubbard model is a highly simplified

attempt at describing the quantum mechanical motion (and behavior in general) of electrons in an actual solid, it displays a range of nontrivial phenomena, such as Mott transition, ferrimagnetism, ferro- and antiferromagnetism, Tomonaga-Luttinger liquid and superconductivity [5].

Within the last couple of years an increasing number of experimental realizations, especially with the use of ultra-cold atoms in optical lattices, made steady progress in probing the model. Details and references to experimental realizations will be given in the second half of chapter four.

The Hubbard Hamiltonian is most generally represented as the sum of a kinetic part and an interaction part

$$\hat{H} \;=\; \hat{H}_{kin} + \hat{H}_{int} \tag{2.10}$$

Neither $\hat{H}_{kin}$ nor $\hat{H}_{int}$ taken on their own favor any long-ranged magnetic ordering. The case of no interaction would lead to a conventional band spectrum with Bloch electrons delocalized over the whole crystal. If we set the hopping term equal to zero and only look at the interaction part, then the Hamiltonian would favor local magnetic moments by suppressing the possibility of doubly occupied sites.
However, their combined sum introduces what Tasaki in his paper called '*a competition between wave-like character and particle-like character (or between linearity and nonlinearity)*' [5], thus giving rise to the various aforementioned phenomena.

The general Hamiltonian in first quantization without external fields reads (cf. e.g. Ref. [20])

$$\hat{H} \;=\; \sum_i \left[-\frac{\hbar^2}{2m_e}\nabla_i^2 + \mathcal{V}(\mathbf{R}_i) \right] + \frac{1}{2}\sum_{i,j} \frac{e^2}{|\mathbf{R}_i - \mathbf{R}_j|} \tag{2.11}$$

with m_e the electron mass, e the elementary charge and $W(\mathbf{R})$ the lattice potential.

Actual atoms have a certain amount of orbitals with electrons in the corresponding states. To describe all possible interactions between different orbitals of different atoms would be an impossible task. Therefore, in the standard Hubbard model the situation is greatly simplified by considering only one non-degenerate orbital state per atom. This can be vindicated with allusion to the range of low energy physics we are interested in, because the electrons in other states have little effect here. Hence the model is also called 'single-orbital' or 'single-band' Hubbard model.

The general Hamiltonian in second quantized form is given by

$$\hat{H} \;=\; \sum_{\sigma}\sum_{i,j} t_{ij}\; c^{\dagger}_{i,\sigma} c_{j,\sigma} + \sum_{\sigma,\sigma'}\sum_{i,j,l,m} U_{ijlm}\; c^{\dagger}_{i,\sigma} c^{\dagger}_{j,\sigma'} c_{l,\sigma'} c_{m,\sigma} \tag{2.12}$$

The hopping amplitude may be written as

$$t_{ij} \;=\; \int d^3r\; w^*(\mathbf{r}-\mathbf{R}_i) \left[-\frac{\hbar^2}{2m_e}\nabla_{\mathbf{r}}^2 + \mathcal{V}(\mathbf{r}) \right] w(\mathbf{r}-\mathbf{R}_j) \tag{2.13}$$

and the electron-electron correlations are

$$U_{ijlm} \;=\; \int\int d^3r\; d^3r'\; w^*(\mathbf{r}-\mathbf{R}_i) w^*(\mathbf{r}'-\mathbf{R}_j)\; \frac{e^2}{|\mathbf{r}-\mathbf{r}'|}\; w(\mathbf{r}'-\mathbf{R}_l) w(\mathbf{r}-\mathbf{R}_m) \tag{2.14}$$

The short-ranged Coulomb interaction U_{ijlm} in its general form represents a four-center integral which is reduced to a direct interaction between two particles by concentrating on the largest

contributions. In metals with a significant DOS at the Fermi level, the Coulomb potential is screened and decays exponentially with distance from the nucleus

$$\mathcal{V}(r) \;=\; \frac{e^{r\lambda}}{r} \tag{2.15}$$

with λ marking the screening length, which for d-electrons is roughly of the size of the Bohr radius a_0 [21].
This justifies a reduction to considering on-site interactions only, i.e. taking into account the most significant elements $U_{iiii} \equiv U$ and disregarding all others.
U mimics a screened Coulomb repulsion among electrons belonging to the same atomic site or, in terms of energy, U is the amount of energy one has to pay when putting two electrons of opposite spin at the same site.

Since the electronic functions are highly located at their 'parent' atom, the nearest-neighbor hopping terms contribute by far the most to the kinetic energy and it is thereby justified to neglect all other hopping processes. Thus we are left with hopping elements $t_{i,i+1} \equiv -t$.

In the case of $t = 0$ all singly occupied states are degenerate. Enabling hopping processes removes the degeneracy and lowers the energy of an antiferromagnetic pair of electrons on neighboring sites relative to a ferromagnetic pair.
Large values of t result in a broad band structure whereas a small t leads to narrow bands.

Hence, we obtain the celebrated Hubbard Hamiltonian

$$\hat{H} \;=\; -t \sum_{\langle i,j\rangle,\sigma} c^{\dagger}_{i,\sigma} c_{j,\sigma} \;+\; U \sum_{i} n_{i\uparrow} n_{i\downarrow} \;-\; \mu \sum_{i,\sigma} n_{i,\sigma} \tag{2.16}$$

where $\langle i,j\rangle$ stands for a summation over neighboring lattice sites, including matrix elements that couple the lattice sites at the edges to satisfy periodic boundary conditions (pbc).
The chemical potential μ is added for the equilibrium Hamiltonian to determine the level of occupation in the initial state. When the system is driven out of equilibrium, there will be no well defined chemical potential.

The energy scale for the simple Hubbard model which basically enters into every physical quantity is determined by the ratio U/t. For convenience we will keep the hopping strength fixed at $t = 1$ and vary only the Coulomb interaction strength U in the numerical calculations.

2.2.1 The one-dimensional chain

We consider a periodic lattice in one dimension, that is a chain of atoms forming a ring. For a detailed discussion of the one-dimensional Hubbard model see [22] and references therein.
Only in 1D the Hubbard model can be solved analytically where an exact solution can be obtained by putting forth the Bethe ansatz technique. All other analytical methods are based on approximations. Using the Bethe ansatz [23] Lieb and Wu [24] were able to compute the 1D ground state and determine that the solution is unique for the half-filled band.

The Hubbard model in 1D describes an insulator for all $U > 0$. Lieb and Wu found that the ground state exhibits no conducting-insulating (Mott) transition when the interaction strength is varied, except at $U = 0$ where the system behaves like a metal. It is only with higher dimensionality that

a Mott transition occurs at some critical value $U_c > 0$. The characteristics of a Mott insulator are discussed in more detail in Sec. 4.4

2.2.2 Representation of the Hilbert space

For this section we follow roughly the general descriptions given in standard books such as Refs. [4, 11, 12].
The dimensionality of the Hilbert space is determined by the number of basis states. In the case of a fermionic system, the total Hilbert space is of dimension 4^Λ (where Λ is the total number of lattice sites), since each site can be empty, singly occupied by either one spin $\uparrow$ or one spin $\downarrow$ electron, or doubly occupied by electrons of opposite spin.
Note that the Hilbert space of a single-particle problem increases linearly with system size, while for a many-body problem it grows exponentially.

Since the fermionic spin S^z is a conserved quantity, i.e. $[\hat{H}, \hat{S}^z] = 0$, the total numbers of spin up (spin down) electrons $N_\uparrow$ ($N_\downarrow$) are good quantum numbers. Consequently, the eigenstates are labelled in occupation number representation.

The anti-commutation relations (2.8) have built into them Pauli's exclusion principle that no two particles may have the same set of quantum numbers. However, care has to be taken when it comes to ordering of the operators. Every exchange of two operators with different site and/or spin indices introduces an additional minus sign, e.g. $c^\dagger_{1\sigma} c^\dagger_{2\sigma}|0\rangle = -c^\dagger_{2\sigma} c^\dagger_{1\sigma}|0\rangle$. The way of ordering the fermionic operators can be chosen arbitrarily but after choosing a particular convention one has to stick to it rigorously throughout all following calculations.

The following two rules are commonly used in second quantization: (i) put all spin up operators to the left of all spin down operators, (ii) arrange the operators with ascending site indices from left to right. For example $c^\dagger_{1\uparrow} c^\dagger_{3\uparrow} c^\dagger_{1\downarrow} c^\dagger_{2\downarrow}|0\rangle$ would be in correct order.

Rule (i) is convenient because with $\hat{N}_\uparrow = \sum_i n_{i\uparrow}$ and $\hat{N}_\downarrow = \sum_i n_{i\downarrow}$ follows that their commutators with the Hamiltonian vanish, that is

$$\left[\hat{H}, \hat{N}_\uparrow\right] \;=\; \left[\hat{H}, \hat{N}_\downarrow\right] \;=\; 0 \;=\; \left[\hat{H}, \hat{N}\right] \tag{2.17}$$

This means that spin up and spin down sectors in the Hilbert space do not mix. Exploiting the fact that the Hamiltonian commutes with the number operator one can restrict the Hilbert space to a particular subspace where the total particle number as well as the particle numbers corresponding to individual spins are fixed.
Rule (ii) follows naturally from labelling the lattice sites with increasing indices. (Another common way would be to apply an ordering with descending indices from left to right.)

From these symmetries ensues that the Hamiltonian is blockdiagonal in $\hat{S}^z$ and $\hat{N}$ and the corresponding sectors in the full Hilbert space can be treated separately.

2.3 The Falicov-Kimball model

This very brief mentioning of the Falicov-Kimball (FK) model is intended to provide only some methodological basics for the data that is used in Chap. 5 in comparison with our results from the Hubbard model.

The FK model involves two sorts of spinless electrons and, in contrast to the Hubbard model, does not favor SU(2) symmetry. The itinerant (conduction band) electrons are able to hop through the lattice, whereas the localized (valence band) electrons do not move but interact with the itinerant electrons by way of a screened Coulomb interaction U when they both occupy the same lattice site. Considerable progress has been made on solving this model with mean-field approaches in equilibrium, where essentially all properties of the conduction electrons are known [9, 25].
For a detailed review of the model and its properties see Ref. [26].

The FK-Hamiltonian is given by

$$\hat{H} = -t \sum_{\langle i,j \rangle} (c_i^\dagger c_j + c_j^\dagger c_i) - \mu \sum_i c_i^\dagger c_i + U \sum_i w_i c_i^\dagger c_i + E \sum_i w_i \tag{2.18}$$

The case $U = 0$ resembles the noninteracting Hubbard model for a single spin species with energies shifted by some constant $(E \cdot N_w)$ that results from the number of localized electrons in the system.

Here the operators $c_i^\dagger$ (c_i) describe the creation (annihilation) of a conduction electron at site i and w_i, being the number operator for localized electrons at site i, is restricted to 0 or 1.

As Freericks points out in his paper [27], the spinless FK model is only weakly dependent on the dimensionality d, the correction being proportional to $1/d$. This makes the model very susceptible to a treatment with Dynamical Mean Field Theory (DMFT) which is usually carried out in the limit of infinite dimensions.

Chapter 3

CPT and pseudoparticle approach

Over the course of the last two decades many numerical methods have become available for the investigation of strongly correlated bosonic and fermionic systems. Among the most common techniques are exact diagonalization (ED), Quantum Monte Carlo methods (QMC) [28], Density-Matrix Renormalization Group (DMRG) [29], Dynamical Mean-Field Theory (DMFT) [30] and various cluster approaches. We will concentrate on the latter and especially on Cluster Perturbation Theory (CPT).

CPT can treat much larger systems than ED and is therefore capable of representing the thermodynamic limit in a better way. In the limit of an infinitely large cluster CPT is equivalent to ED.

DMFT will also play a role in chapter five where we will compare our numerical results obtained by CPT with data from DMFT-calculations. In contrast to CPT which considers small systems, DMFT works in the thermodynamic limit of an infinitely large system and becomes exact in the limit of infinite dimensions. On the other hand, in lower dimensions DMFT is quite a strong approximation since spatial correlations are neglected altogether. This fact can be partially remedied by considering small clusters instead of single impurity sites surrounded by a thermodynamic bath. Such cluster-treatment generalizations of DMFT are incorporated in Cluster-DMFT (C-DMFT) [31] and Dynamical Cluster Approximation (DCA) [32] methods. CPT and C-DMFT in turn can be considered special cases of a more general method, the so-called Self-Energy Functional Approach (SFA) [33] which was proposed only a few years ago.

The main difference between CPT and C-DMFT is that in the case of CPT the intra-cluster hopping strength is fixed and one has no variational parameters at hand. With C-DMFT an additional hopping to correlated bath sites is introduced that acts as a variational parameter.
An intermediate approach between CPT and DMFT is Variational Cluster Perturbation Theory (V-CPT, also called Variational Cluster Approach, VCA) where additional one-particle operators are included into the cluster Hamiltonian and subsequently subtracted again in the perturbative part of the Hamiltonian. This for instance provides for the inclusion of symmetry-breaking fields and other variational parameters in the model. Symmetry-broken phases are not allowed in CPT because it does not favor any kind of self-consistency procedure. (For a detailed discussion of V-CPT see in particular Ref. [2].)

In C-DMFT the bath of uncorrelated sites can exchange electrons with the cluster and the bath parameters are determined self-consistently. The Hubbard Hamiltonian stated in (2.16) takes on the following form [34] embodying an Anderson impurity model

$$\hat{H} \;=\; -t \sum_{\langle m,n \rangle} c_m^\dagger c_n + U \sum_m n_{m\uparrow} n_{m\downarrow} + \sum_{m,\nu} \theta_{m\nu} \left(c_m^\dagger a_\nu + \text{h.c.} \right) + \sum_\nu \epsilon_\nu a_\nu^\dagger a_\nu \tag{3.1}$$

where ν labels bath orbitals with energy ϵ_ν, a_ν annihilates an electron at bath site ν, $\theta_{m\nu}$ is the bath-cluster hybridization matrix and explicit spin indices have been omitted.

3.1 The CPT procedure

Cluster Perturbation Theory [35] can be understood as a cluster extension of strong-coupling perturbation theory [36] limited to lowest order but where the starting point is a cluster instead of a single site.
The first approximation is that we are dealing with an ideal crystal, i.e. a lattice without disorder, impurities or distortions of any kind. Furthermore, instead of taking into account the full crystal lattice, one breaks up the lattice into separate clusters of a certain size and shape. This means that by choosing a particular cluster tiling the full lattice Hamiltonian $\hat{H}$ is split into a cluster part $\hat{H}_0$ which contains everything that is going on inside the cluster and a part $\hat{V}$ that deals with interactions (i.e. hopping terms) between the clusters. Thereby the original dynamics of the lattice is recovered and the non-relativistic many-body Hamiltonian in the absence of external fields takes on the general form

$$\hat{H} \;=\; \hat{H}_0 + \hat{V} \tag{3.2}$$

where

$$\hat{H}_0 \;=\; \sum_a \left[-t \sum_{n,m,\sigma} c^\dagger_{n,a;\sigma} c_{m,a;\sigma} \;+\; U \sum_{m,a\sigma} n_{m,a;\uparrow} n_{m,a;\downarrow} \;-\; \mu \sum_{m,\sigma} n_{m,a;\sigma} \right] \tag{3.3}$$

is treated exactly and

$$\hat{V} \;=\; \sum_\sigma \sum_{a,b} \sum_{n,m} \mathrm{V}_{nm,ab}\; c^\dagger_{n,a;\sigma} c_{m,b;\sigma} \tag{3.4}$$

designates the perturbation. Here a, b label the clusters and n, m represent sites inside one of these clusters.

For the calculation of the matrix elements, eigenstates, etc. of the intra-cluster Hamiltonian $\hat{H}_0$ we imply open boundary conditions. However, for the whole lattice we will use periodic boundary conditions, thus connecting for example site 1 with site Λ in the one-dimensional chain which is equivalent to putting $\Lambda + 1 = 1$ for sites as well as $N_c + 1 = 1$ for clusters in the corresponding sums. CPT in principle does not favor any particular choice of boundary conditions. But since we want to measure a current flowing through the lattice, open boundary conditions would lead to an accumulation of particles on one edge of the crystal lattice.

The cluster decomposition of the full lattice consisting of Λ sites into N_c clusters of size L breaks the translational invariance of the original lattice. In the interest of recovering the lost symmetry a periodization procedure of the Green function is put into action [34].
By coupling the clusters within strong-coupling perturbation theory the Green function in the thermodynamic limit is recovered.

In order to obtain the single cluster energies we need to solve the eigenvalue problem of the Hamiltonian given in (3.2). Basically, an explicit construction of the Hamiltonian matrix is needed to represent the action of the Hamiltonian on the state vectors.

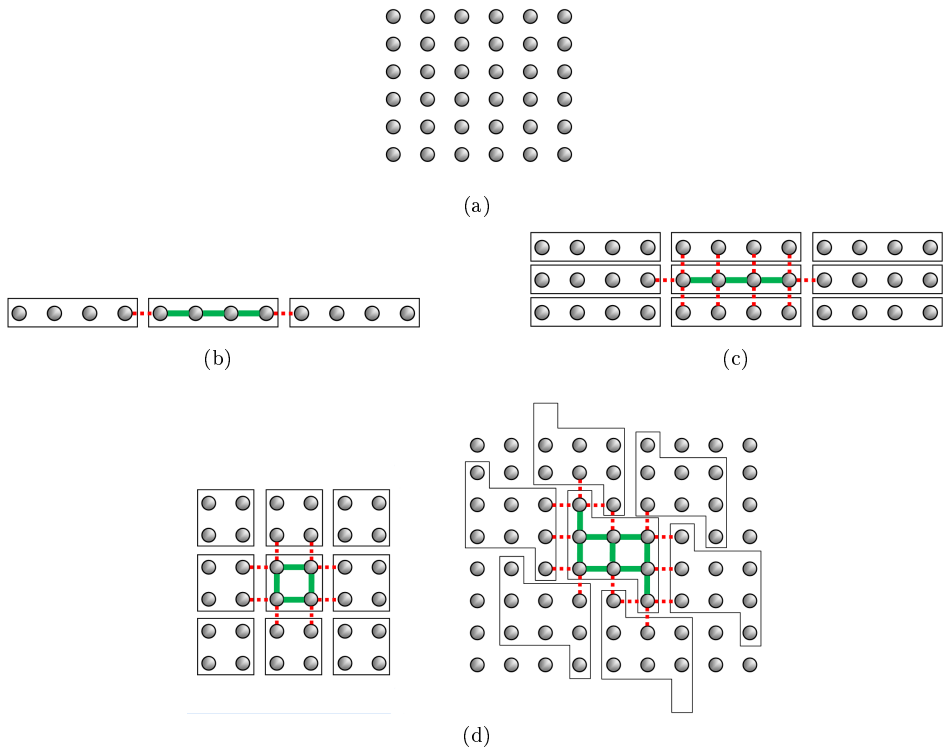

Figure 3.1: Examples of different lattice tilings: (a) original lattice; (b) 1D tiling with four sites per cluster; (c) semi-2D tiling with one-dimensional clusters coupled together; (d) 2D cluster tiling of size 2x2 and $\sqrt{8}$x$\sqrt{8}$ respectively. In 2D variety of different sizes and shapes is imaginable, every site has 4 nearest neighbors. Depending on the tiling the hoppings are treated either exactly (within the cluster, indicated in green) or perturbatively (across cluster boundaries, red).

The ground state is found either by direct diagonalization (for very small cluster sizes) or by iterative methods, such as Lanczos or band Lanczos algorithms that can deal with cluster sizes up to 16 sites.

A treatment of CPT with respect to Green functions is included in the appendix.

Reciprocal space

Associated with each site $(a, b, \dots)$ of the superlattice Γ is a cluster consisting of L sites labeled $(n, m, \dots)$. The position of each site of the full lattice γ can be expressed as a combination of a cluster vector plus a vector inside the cluster, such that $\mathbf{R}_i = \mathbf{R}_a + \mathbf{r}_n$.
Accordingly, the wave vectors that constitute the Brillouin zone BZ_γ of the total lattice can be expressed in terms of wave vectors $\tilde{\mathbf{k}}$ belonging to the Brillouin zone BZ_Γ of the superlattice and wave vectors $\mathbf{K}$ of the reciprocal superlattice that also belong to BZ_γ

$$\mathbf{k} \;=\; \tilde{\mathbf{k}} + \mathbf{K} \tag{3.5}$$

In Fig. 3.1 the example of a 2D lattice split into 2x2 clusters is illustrated on the left hand side of panel (d).

The passage from real space to momentum space via full Fourier transformation ($i \leftrightarrow \mathbf{k}$) is equivalent to carrying out two partial transforms

$$\begin{aligned} \mathcal{O}_a &= \frac{1}{\sqrt{N_c}} \sum_{\tilde{\mathbf{k}}} e^{\mathrm{i}\,\tilde{\mathbf{k}}\mathbf{R}_a} \mathcal{O}_{\tilde{\mathbf{k}}} \\ \mathcal{O}_n &= \frac{1}{\sqrt{L}} \sum_{\mathbf{K}} e^{\mathrm{i}\,\mathbf{K}\mathbf{r}_n} \mathcal{O}_{\mathbf{K}} \end{aligned} \tag{3.6}$$

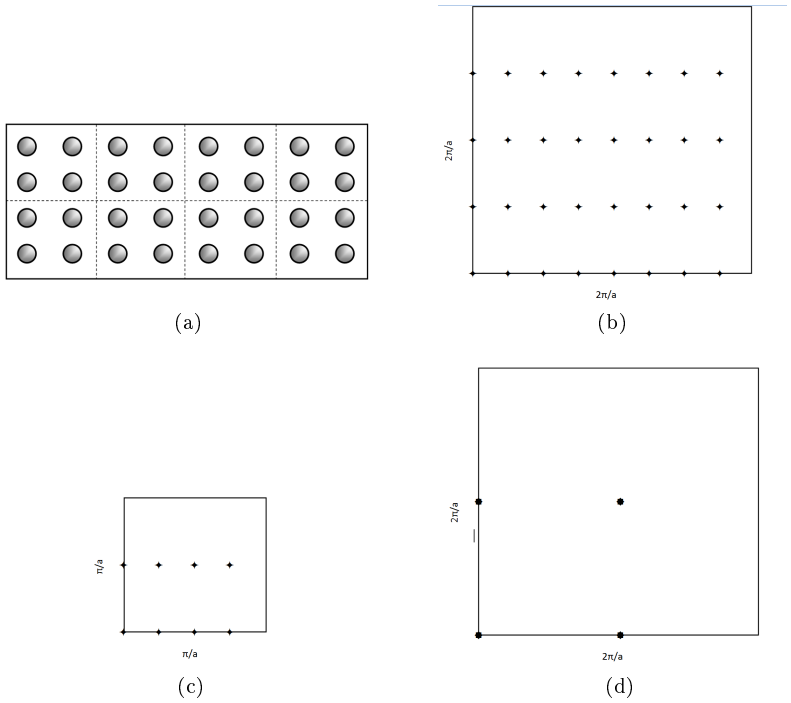

(a) (b) (c) (d)

Figure 3.2: Fourier transformations: (a) full lattice γ in real space, (b) full lattice in reciprocal space (BZ_γ), (c) BZ_Γ of the reciprocal superlattice, (d) Brillouin zone of one cluster providing additional reciprocal lattice vectors to complete the full reciprocal vector space.

In the example given in Fig. 3.2 we have a lattice of 32 sites split into eight 2x2 clusters.
The full reciprocal lattice consists of crystal momenta $k_x = \frac{\pi}{4a}\{0, 1, \ldots, 7\}$ and $k_y = \frac{\pi}{2a}\{0, \ldots, 3\}$ where a denotes the lattice constant. The Brillouin zone of the superlattice BZ_Γ is reduced due to the cluster size to $\tilde{k}_x = \frac{\pi}{4a}\{0, \ldots, 3\}$ and $\tilde{k}_y = \frac{\pi}{2}\{0, 1\}$. In combination with the reciprocal cluster vectors $K_{x,y} = \frac{\pi}{a}\{0, 1\}$ the full Brillouin zone BZ_γ is recovered.
Note that each Brillouin zone contains a complete and irreducible set of wave vectors.

3.2 Pseudoparticle approach

This section is based on the considerations leading to the CPT expression for the Green function as it has been laid out in Ref. [10]. The authors show that the CPT formalism is equivalent to

a mapping onto a model of hard-core fermions which describe single-particle excitations from the cluster's ground state.

The excited states are generated by creating or annihilating one particle in the ground state

$$\begin{aligned} c^\dagger|GS\rangle &= |\alpha\rangle \\ c\ |GS\rangle &= |\beta\rangle \end{aligned} \tag{3.7}$$

We diagonalize the Hamiltonian (3.3) corresponding to the single cluster and find its ground state $|GS\rangle$ with energy set to zero, i.e. $\epsilon_{GS} = 0$, and a total number of N particles. By labelling the excited states $|\alpha\rangle$ for states that comprise $N+1$ electrons and $|\beta\rangle$ for states containing $N-1$ electrons, one can define creation operators $d_\gamma^\dagger$ and annihilation operators d_γ such that

$$\begin{aligned} d_\gamma^\dagger|GS\rangle &= |\gamma\rangle \\ d_\gamma|\gamma\rangle &= |GS\rangle \end{aligned} \tag{3.8}$$

where $\gamma = \{\alpha, \beta\}$.

The transition matrix elements are given by

$$\begin{aligned} \mathrm{T}^*_{n\alpha} &= \langle\alpha|c_n^\dagger|GS\rangle &= \langle GS|c_n|\alpha\rangle^* \\ \mathrm{S}^*_{n\beta} &= \langle GS|c_n^\dagger|\beta\rangle &= \langle\beta|c_n|GS\rangle^* \end{aligned} \tag{3.9}$$

Throughout the following it is assumed that the hard-core constraint

$$\sum_\gamma d_\gamma^\dagger d_\gamma \leq 1 \tag{3.10}$$

is satisfied.

Expressing the original fermionic operators $c_n^\dagger$ and c_n in terms of the new operators d_γ yields

$$c_n^\dagger = \sum_\alpha \mathrm{T}^*_{n\alpha} d_\alpha^\dagger + \sum_\beta \mathrm{S}^*_{n\beta} d_\beta \tag{3.11}$$

Since the intra-cluster Hamiltonian is diagonal in the d operators, $\hat{H}_0$ can be rewritten as

$$\hat{H}_0 = \sum_{\sigma,a,\gamma} \epsilon_\gamma d^\dagger_{\gamma,a} d_{\gamma,a} \tag{3.12}$$

Here, $\epsilon_\alpha = E_\alpha - E_0$ denote the excitation energies with respect to the ground state energy E_0. The diagonalization has no immediate effect on the inter-cluster Hamiltonian $\hat{V}$ as it was given in (3.4).

In the next step we perform the following particle-hole transformation

$$\begin{aligned} p_\alpha^\dagger &= d_\alpha^\dagger \\ p_\beta^\dagger &= d_\beta \end{aligned} \tag{3.13}$$

The transition matrix elements from (3.9) can be combined in a single rectangular matrix Q such that

$$\begin{aligned} \mathrm{Q}_{n\alpha} &= \mathrm{T}_{n\alpha} \\ \mathrm{Q}_{n\beta} &= \mathrm{S}_{n\beta} \end{aligned} \tag{3.14}$$

The corresponding transformation of the fermionic operators from (3.11) then takes on the form

$$c_n^\dagger = \sum_\gamma p_\gamma^\dagger \, \mathrm{Q}_{\gamma n}^* \tag{3.15}$$

and accordingly

$$c_n = \sum_\gamma \mathrm{Q}_{n\gamma} \, p_\gamma \tag{3.16}$$

And the inverse transformation returns

$$\begin{aligned} p_\gamma^\dagger &= \sum_n c_n^\dagger \, Q_{n\gamma} \\ p_\gamma &= \sum_n Q_{\gamma n}^* \, c_n \end{aligned} \tag{3.17}$$

This changes the intra-cluster Hamiltonian to

$$\hat{H}_0 = \sum_{\sigma,a,\gamma} \eta_\gamma \epsilon_\gamma p_{\gamma,a}^\dagger p_{\gamma,a} \tag{3.18}$$

where η_γ represents the appropriate sign accompanying the $N+1$ and $N-1$ states respectively

$$\eta_\gamma = \begin{cases} +1 & \text{if } |\gamma\rangle = |\alpha\rangle \\ -1 & \text{if } |\gamma\rangle = |\beta\rangle \end{cases} \tag{3.19}$$

From now on we will use the indices α, β and γ generally for all pseudoparticle states since the distinction with regard to particle number is no longer necessary.

3.2.1 Perturbation $\hat{V}$

In order to keep the following calculations simple, we will reduce our considerations for the moment to a one-dimensional system. The extension to 2D is straightforward.
The intra-cluster part $\hat{V}$ of the Hamiltonian describes nearest-neighbor hopping processes between adjacent clusters and has the form of a one-body operator, which in 1D (cf. Ref. [35]) reads as

$$\hat{V}_{mn,ab} = -t \left[\delta_{a,b-1} \delta_{m,L} \delta_{n,1} + \delta_{a,b+1} \delta_{m,1} \delta_{n,L} \right] c_{m,a}^\dagger c_{n,b} \tag{3.20}$$

This exemplifies the hopping between the first and the last lattice site of two neighboring clusters

$$\hat{V}_{mn,aa+1} = -t \left[c_{L,a}^\dagger c_{1,a+1} + c_{1,a}^\dagger c_{L,a-1} \right] \tag{3.21}$$

The reciprocal superlattice representation of the matrix elements is given by the partial Fourier transform

$$\mathrm{V}_{mn,\tilde{\mathbf{k}}} \;=\; \sum_{\mathbf{R}_a} \mathrm{V}_{mn,aa+1} e^{\mathrm{i}\,\tilde{\mathbf{k}}\mathbf{R}_a} \tag{3.22}$$

$\hat{V}$ is now given in a mixed representation: reciprocal space for the superlattice cluster-sites and real space for the atomic sites inside each single cluster.

In terms of the pseudoparticle formulation the intra-cluster Hamiltonian becomes

$$\hat{V} \;=\; \sum_{\sigma} \sum_{a,b} \sum_{\alpha,\beta} \sum_{n,m} \mathrm{V}_{nm,ab}\; \mathrm{Q}^{*}_{\alpha n}\; \mathrm{Q}_{m\beta}\; p^{\dagger}_{\alpha,a}\; p_{\beta,b} \tag{3.23}$$

3.2.2 Pseudoparticle Hamiltonian

The total Hamiltonian (3.2) combining inter- and intra-cluster terms can be written as

$$\hat{H} \;=\; \sum_{\sigma} \sum_{a,b} \sum_{\alpha,\beta} p^{\dagger}_{\alpha,a}\; \mathrm{h}_{\alpha\beta,ab}\; p_{\beta,b} \tag{3.24}$$

The above pseudoparticle Hamiltonian describes the hopping of pseudoparticles between adjacent clusters with amplitudes

$$\mathrm{h}_{\alpha\beta,ab} \;=\; \delta_{\alpha\beta}\epsilon_{\alpha}\eta_{\alpha} + \left(\mathrm{Q}^{\dagger}\mathrm{V}_{ab}\mathrm{Q}\right)_{\alpha\beta} \tag{3.25}$$

The Hamiltonian is bilinear in creation and annihilation operators. In principle a Hamiltonian of this form can always be solved by diagonalization of the corresponding matrix. This property will be very useful when evaluating expectation values (see Sec. 3.6).

Multiple particle excitations from the clusters' ground state are ignored. Note that $\mathrm{Q}\mathrm{Q}^{\dagger} = 1$ but $\mathrm{Q}^{\dagger}\mathrm{Q} \neq 1$ since Q is not a square matrix.

The main benefit from this calculation is the fact that the lattice Hamiltonian (3.24) now consists only of one-particle operators whereas the original Hamiltonian (3.3) due to on-site interactions included two-particle operators as well.

Pseudoparticle Green function

As a side note we will briefly touch on the subject of Green functions because of their importance for calculating expectation values that can be compared to experimental results. The appendix contains in a nutshell the full CPT Green function formalism. However, for our purposes only the total Green function expressed in pseudoparticle operators p shall be mentioned here

$$\langle\langle p_{\alpha,a}, p^{\dagger}_{\beta,b}\rangle\rangle \;=\; \left(\mathrm{i}\,\omega - \mathrm{h}\right)^{-1}_{\alpha\beta,ab} \tag{3.26}$$

Accordingly, in terms of the bare fermionic operators the Green function has the form

$$\langle\langle c_{n,a}, c^{\dagger}_{m,b}\rangle\rangle \;=\; \mathrm{Q}_{n\alpha}\; \langle\langle p_{\alpha,a}, p^{\dagger}_{\beta,b}\rangle\rangle\; \mathrm{Q}^{*}_{\beta m} \tag{3.27}$$

which in matrix notation may be expressed as

$$\langle\langle \mathbf{c}_a, \mathbf{c}_b^\dagger \rangle\rangle \;=\; \Big[\mathrm{Q} \big(\mathrm{i}\,\omega - \mathrm{h} \big)^{-1} \mathrm{Q}^\dagger \Big]_{ab} \tag{3.28}$$

3.3 Peierls' substitution

The considerations so far were mainly based on what has been established in pertinent literature and papers concerning the fundamentals of CPT. We will now proceed to introduce and incorporate an external electric field into the formalism with the aid of Peierls' substitution and then carry on to develop a scheme for the time evolution of the system in Sec. 3.4.

The electric field is applied along the x-direction, that is, parallel to the 1D lattice vector. In general an electric field is described by means of a scalar potential $\Phi(\mathbf{r},\tau)$ and a vector potential $\mathbf{A}(\mathbf{r},\tau)$

$$\mathbf{E}(\mathbf{r},\tau) \;=\; -\nabla\Phi(\mathbf{r},\tau) - \frac{1}{c}\frac{\partial \mathbf{A}(\mathbf{r},\tau)}{\partial \tau} \tag{3.29}$$

We consider the case where the electric field is turned on at time $\tau = 0$ and furthermore ignore all relativistic effects.

The electric field remains invariant under the simultaneously performed gauge transformations $\mathbf{A} \to \mathbf{A} + \nabla\chi$ and $\Phi \to \Phi - \frac{\partial\chi}{\partial\tau}$. This mathematical degree of freedom allows us to choose a gauge that fits the problem at hand. Thus, we shall set

$$\Phi(\mathbf{r},\tau) = 0 \tag{3.30}$$

which is sometimes called the Hamiltonian or Landau gauge.

The Hubbard Hamiltonian in (2.16) is time independent. In order to include the effect of the vector potential we perform a Peierls' substitution [37, 38] where a phase factor is added to the original hopping matrix, yielding

$$t \;\longrightarrow\; t \exp\left[-\frac{\mathrm{i}\,e}{\hbar c} \int_{\mathbf{R}_i}^{\mathbf{R}_j} d^3r \; \mathbf{A}(\mathbf{r},\tau) \right] \tag{3.31}$$

The Peierls phase can be derived from Feynman diagrams or from 'brute force' calculations of $\langle w_i | \hat{H} | w_j \rangle$ where w_i are Wannier functions and the Hamiltonian in first quantized form, as an extension of (2.11), is given by

$$\hat{H} \;=\; \sum_i \left[\frac{\hbar^2}{2m_e} \left(-\mathrm{i}\,\nabla_i - \frac{e\mathbf{A}(\mathbf{R}_i,\tau)}{\hbar c} \right)^2 + \mathcal{V}(\mathbf{R}_i) \right] + \frac{1}{2} \sum_{i,j} \frac{e^2}{|\mathbf{R}_i - \mathbf{R}_j|} \tag{3.32}$$

Without exercising a full derivation, a brief motivation using Feynman path integrals would amount to the following: The transition amplitude $\langle \mathbf{x}', \tau' | \mathbf{x}, \tau \rangle$ for a general state at time τ to a state at time τ' is characterised by the weighting factor $\exp(\mathrm{i}\,\frac{e}{\hbar c}\mathrm{S}[\mathbf{x}(\tau)])$ where the action S is the integral over time of the Lagrange function. The Lagrange function for the free electromagnetic field is

given by $\mathrm{L} = \frac{1}{2}m\mathbf{v}^2 - e\Phi(\mathbf{x}) + \frac{e}{c}\mathbf{A}\cdot\mathbf{v}$. When inserting this in the path integral, the last term of the Lagrangian results in the aforementioned Peierls phase factor.

It is difficult to assimilate the magnetic field that is associated with the vector potential in the present description, so it would be convenient to find a reasonable way to forget about it altogether. We are interested in electric fields that are affecting the atomic system in a general and ideally uniform way. That is, the spatial dependence of the electric field is supposed to be very weak. This means for the magnetic field that it is sufficiently small to be left out of our considerations [38]. Still, one has to be aware of this approximation because after all it implies that our electromagnetic field does no longer satisfy Maxwell's equations, unless the field, besides being uniform in space, is also constant in time.
Such conditions can be experimentally realized in nanostructures where the applied potential creates a nearly homogeneous E-field due to the small size of the system [39].

Hence, we neglect the spatial dependence of the vector potential and consider an electric field that is uniform in space. With the vector potential being homogeneous we assume that the effects of the magnetic field can be neglected, since the magnetic field would be given by the curl of $\mathbf{A}(\mathbf{r},\tau)$. However, there are no restrictions on whether $\mathbf{E}$ is constant or varying in time.
Note, by considering a single-band model we also ignore dipole or multipole transitions between different bands.

With $\mathbf{A}(\mathbf{r},\tau) \equiv \mathbf{A}(\tau)$ and taking $c = 1$, the electric field becomes

$$\mathbf{E}(\tau) \;=\; -\frac{\partial \mathbf{A}(\tau)}{\partial \tau} \tag{3.33}$$

The time dependent Hamiltonian for interacting electrons in second quantization including the chemical potential has the form (cf. equation (2.16))

$$\hat{H} \;=\; -t \sum_{\langle i,j\rangle,\sigma} \exp\left(-\frac{\mathrm{i}\, e}{\hbar c} \int_{\mathbf{R}_i}^{\mathbf{R}_j} d^3r\; \mathbf{A}(\tau) \right) c^\dagger_{i,\sigma} c_{j,\sigma} \;+\; U \sum_i n_{i\uparrow} n_{i\downarrow} \;-\; \mu \sum_{i,\sigma} n_{i,\sigma} \tag{3.34}$$

The spatial integration within the Peierls phase factor is readily carried out, resulting in

$$t \;\longrightarrow\; t e^{-\mathrm{i}\,\mathbf{A}\cdot(\mathbf{R}_j - \mathbf{R}_i)} \tag{3.35}$$

The electric field is treated as an external perturbation that is turned on at time $\tau = 0$. This means that the ground state is unaffected and the Hamiltonian changes to

$$\hat{H}(\tau) \;=\; \hat{H}_0 + \hat{H}_0^A(\tau) + \hat{V}^A(\tau) \;=\; \hat{H}_0 + \hat{V}(\tau) \tag{3.36}$$

The additional term $\hat{H}_0^A(\tau)$ pays tribute to the effects of the electric field inside the cluster. Since the cluster has been diagonalized at $\tau = 0$, the hopping terms contributing to $\hat{H}_0$ must be subtracted again in $\hat{H}_0^A(\tau)$. This implies that the transition elements for $\hat{H}_0^A(\tau)$ take on the form

$$t \;\longrightarrow\; t\left(e^{-\mathrm{i}\,\mathbf{A}\cdot(\mathbf{R}_j - \mathbf{R}_i)} - 1 \right) \tag{3.37}$$

The sum of the inter-cluster hopping matrix $\hat{V}^A(\tau)$ and the amended single cluster part $\hat{H}_0^A(\tau)$ now build up the time dependent perturbation term $\hat{V}(\tau)$ in the full CPT-Hamiltonian as indicated in

(3.36). Thus, the total Hamiltonian may be written symbolically as

$$\hat{H}(\tau) \;=\; \sum_{\sigma} \sum_{\tilde{\mathbf{k}}} p^{\dagger}_{\alpha,\tilde{\mathbf{k}}}(\tau)\; \mathrm{h}_{\alpha\beta,\tilde{\mathbf{k}}}(\tau)\; p_{\beta,\tilde{\mathbf{k}}}(\tau) \tag{3.38}$$

with matrix elements

$$\mathrm{h}_{\alpha\beta,\tilde{\mathbf{k}}} \;=\; \Big(\mathrm{H}_0 + \mathrm{Q}^{\dagger}\mathrm{V}_{\tilde{\mathbf{k}}}(\tau)\mathrm{Q}\Big)_{\alpha\beta} \tag{3.39}$$

The explicit nature of $\mathrm{V}_{\tilde{\mathbf{k}}}(\tau)$ depends both on the appearance of the lattice as well as on the design of the cluster tiling. As an example, the case of a two-dimensional lattice will be demonstrated at the end of this chapter in Sec. 3.5.

3.4 Time evolution

Next we set out to tackle the time evolution of the system. It is convenient to work in the Heisenberg picture of quantum mechanics where the operators are time dependent and thus subject to evolution in time and all the state vectors are not. This especially includes the creation and annihilation operators although their time dependence was not made explicit in the previous manipulations.

The assumption of a linear response to some external perturbation is well justified in cases where the perturbation is small. In recent years experimental conditions have become accessible where the system's response, when it is driven out of equilibrium, cannot be described linearly. For example, the application of very high voltages or strong lasers produce nonlinear effects. The electric field in our case is quite large and a treatment in linear response theory would not only be unjustified but rather erroneous.
Starting from the time dependent Schrödinger equation we will develop a method to iteratively calculate the matrix elements for the time evolution operator from the Hamilton matrix at corresponding times.

3.4.1 Time evolution in the non-linear regime

The time dependent pseudoparticle Hamiltonian in reciprocal space as expressed in (3.38) is quadratic in the creation and annihilation operators $\mathbf{p}^{\dagger}$ and $\mathbf{p}$.

In the Heisenberg picture the operators carry the time dependence, which means that the Hamiltonian may be written as

$$\hat{H}_H \;=\; \hat{U}^{\dagger}(\tau)\hat{H}_S\hat{U}(\tau) \;\equiv\; \hat{H}(\tau) \tag{3.40}$$

where $\hat{H}_S$ indicates the time independent Hamilton operator in the Schrödinger picture (for details see e.g. Refs. [40, 41]).
The time evolution of the state vectors is governed by a unitary propagator (because $\hat{H}$ is hermitian) that can be extracted leaving the states again independent in time. Henceforth the Heisenberg picture is understood whenever time dependence is implied and we again omit the subscript H.

The time evolution operator obeys the following differential equation

$$\mathrm{i}\,\hbar\frac{d\hat{U}(\tau)}{d\tau} \;=\; \hat{H}(\tau)\hat{U}(\tau) \tag{3.41}$$

with the initial condition $\hat{U}(\tau = 0) = 1$.

In order to solve the equation of motion we use the general ansatz $p_\gamma(\tau) = \mathrm{U}_{\gamma\alpha}(\tau)p_\alpha(0)$ where $\mathrm{U}_{\gamma\alpha}$ denote the elements of a time dependent unitary matrix $\mathrm{U}(\tau)$.

Since fermionic operators can easily be a transformed if the anticommutation relations are not violated, which is always the case for unitary transformations, we perform a unitary transformation to make the time dependence of the pseudoparticle operators explicit. Unitary transformations also preserve the norm of the quantum mechanical states.

$$\begin{aligned} p_{\alpha,\tilde{\mathbf{k}}}(\tau) \;&=\; \sum_\gamma \mathrm{U}_{\alpha,\gamma}(\tau)\; p_{\gamma,\tilde{\mathbf{k}}}(0) \\ p^\dagger_{\alpha,\tilde{\mathbf{k}}}(\tau) \;&=\; \sum_\gamma \mathrm{U}^*_{\gamma,\alpha}(\tau)\; p^\dagger_{\gamma,\tilde{\mathbf{k}}}(0) \end{aligned} \tag{3.42}$$

To illustrate in a brief example the fact that the transformed operators again describe fermions we take the unitary transformation $\mathbf{d} = \mathrm{U}\mathbf{f}$, $\mathbf{d}^\dagger = \mathbf{f}^\dagger\mathrm{U}^\dagger$ (and accordingly $\mathbf{f} = \mathrm{U}^\dagger\mathbf{d}$, $\mathbf{f}^\dagger = \mathbf{d}^\dagger\mathrm{U}$) for fermionic vector operators $\mathbf{d}$ and evaluate the anticommutator in matrix notation to proof their fermionic character

$$\begin{aligned} \left\{\mathbf{f},\mathbf{f}^\dagger\right\} \;&= \mathbf{f}\mathbf{f}^\dagger + \left(\mathbf{f}^{\dagger T}\mathbf{f}^T\right)^T \\ &= \mathrm{U}^\dagger\mathbf{d}\mathbf{d}^\dagger\mathrm{U} + \left(\mathrm{U}^T\mathbf{d}^{\dagger T}\mathbf{d}^T\mathrm{U}^{\dagger T}\right)^T \\ &= \mathrm{U}^\dagger\mathbf{d}\mathbf{d}^\dagger\mathrm{U} + \;\mathrm{U}^\dagger\left(\mathbf{d}^{\dagger T}\mathbf{d}^T\right)^T\mathrm{U} \\ &= \mathrm{U}^\dagger\left\{\mathbf{d},\mathbf{d}^\dagger\right\}\mathrm{U} \end{aligned} \tag{3.43}$$

Schrödinger's equation becomes a differential equation for a general, explicitly time dependent operator $\hat{O}(\tau)$ in the Heisenberg picture

$$\frac{d}{d\tau}\hat{O}(\tau) \;=\; \frac{\mathrm{i}}{\hbar}\left[\hat{H}(\tau),\hat{O}(\tau)\right] + \hat{U}^\dagger(\tau)\left(\frac{d}{d\tau}\hat{O}(\tau)\right)\hat{U}(\tau) \tag{3.44}$$

For the pseudoparticle annihilation operators, and analogous the creation operators, which are not explicitly time-dependent, this yields Heisenberg's equation of motion (in atomic units)

$$\frac{d}{d\tau}p_\gamma(\tau) \;\equiv\; \frac{d}{d\tau}\left(\hat{U}^\dagger p_\gamma\hat{U}\right) \;=\; \mathrm{i}\left[\hat{H}(\tau),p_\gamma(\tau)\right] \tag{3.45}$$

A short computation to determine the commutator in the above relation yields

$$\left[\hat{H}(\tau),p_\gamma(\tau)\right] \;=\; \hat{U}^\dagger(\tau)\left[\hat{H},p_\gamma\right]\hat{U}(\tau) \tag{3.46}$$

and furthermore

$$\left[\hat{H},p_\gamma\right] \;=\; -\mathrm{h}_{\gamma\beta}\;p_\beta \tag{3.47}$$

In the second line all quantities are evaluated at time $\tau = 0$ because the time dependence has been pulled out and absorbed by the propagator $\hat{U}(\tau)$.

Putting this into (3.45) and expanding the left-hand side produces the relation

$$\left(\frac{d}{d\tau}\hat{U}^\dagger(\tau)\right) p_\gamma \hat{U}(\tau) + \hat{U}^\dagger(\tau) p_\gamma \left(\frac{d}{d\tau}\hat{U}(\tau)\right) \;=\; -\,\mathrm{i}\,\hat{U}^\dagger(\tau)\Big(\mathrm{h}_{\gamma\beta}\; p_\beta\Big)\hat{U}(\tau) \tag{3.48}$$

and we are finally left with

$$\frac{d}{d\tau} p_\gamma(\tau) \;=\; -\,\mathrm{i}\,\mathrm{h}_{\gamma\beta}\; p_\beta(\tau) \tag{3.49}$$

From (3.38) it can be seen that the crystal momentum $\tilde{\mathbf{k}}$ enters the Hamiltonian only as a parameter and therefore we can treat each superlattice wave vector $\tilde{\mathbf{k}}$ (as is the case with σ) independently, i.e. they do not mix.

3.4.2 The implicit midpoint rule

We are looking for a numerical method that allows us to carry out the evolution over time while (ideally) preserving the unitarity of its propagator, such that $\mathrm{U}\mathrm{U}^\dagger = \mathrm{U}^\dagger\mathrm{U} = 1$ at all times. This is necessary in order for the eigenvalues of the Hamiltonian to remain unchanged whilst the creation and annihilation operators are being evolved in time.
There are quite a lot of elaborate numerical integrators like Runge-Kutta or predictor-corrector methods around. However, as we are particularly concerned about unitarity, we will apply the following implicit midpoint rule [42], which is a variant of the Cranck-Nicholson method, for the propagator's matrix embodiment

$$\frac{\mathrm{U}(\tau_{n+1}) - \mathrm{U}(\tau_n)}{\Delta\tau} \;=\; \mathrm{i}\,\frac{1}{2}\mathrm{H}(\tau_{n+\frac{1}{2}})\big[\mathrm{U}(\tau_{n+1}) + \mathrm{U}(\tau_n)\big] \tag{3.50}$$

$\Delta\tau$ represents the discrete time step with $\tau_n = n\Delta\tau$ and $\tau_{n+\frac{1}{2}} = \frac{1}{2}(\tau_n + \tau_{n+1})$.

This can be rearranged into

$$\left[1 + \frac{\mathrm{i}\,\Delta\tau}{2}\mathrm{H}(\tau_{n+\frac{1}{2}})\right]\mathrm{U}(\tau_{n+1}) \;=\; \left[1 - \frac{\mathrm{i}\,\Delta\tau}{2}\mathrm{H}(\tau_{n+\frac{1}{2}})\right]\mathrm{U}(\tau_n) \tag{3.51}$$

yielding a recursive expression for the propagator

$$\mathrm{U}(\tau_{n+1}) \;=\; \frac{1 + \frac{i\Delta\tau}{2}\mathrm{H}(\tau_{n+\frac{1}{2}})}{1 - \frac{\mathrm{i}\,\Delta\tau}{2}\mathrm{H}(\tau_{n+\frac{1}{2}})}\;\mathrm{U}(\tau_n) \tag{3.52}$$

3.5 A lattice in 2D

With the considerations laid out in the previous sections, we now have the necessary tools at hand to turn our attention back to the lattice model and execute these methods on a particular system. For the two-dimensional lattice we use a rectangular cluster tiling with at least two sites in each direction. The simplest realization would be the quadratic 2x2 cluster as depicted in the left panel of Fig. 3.1(d). The total number of lattice sites can in principle be chosen arbitrarily and is only limited by computational resources. However, periodic boundary conditions demand it to be a multiple of the cluster size for every direction.

The full reciprocal lattice takes on the shape of a rectangle if the cluster tiling has maximal symmetry, such that the unit cell of the superlattice consists only of a single cluster. The basis vectors in reciprocal space are chosen parallel to the superlattice vectors in real space

$$\tilde{\mathbf{k}} \;=\; \tilde{k}_x \hat{\mathbf{a}}_\Gamma + \tilde{k}_y \hat{\mathbf{b}}_\Gamma \tag{3.53}$$

where $\hat{\mathbf{a}}_\Gamma = \frac{\mathbf{a}_\Gamma}{|\mathbf{a}_\Gamma|}$, $\hat{\mathbf{b}}_\Gamma = \frac{\mathbf{b}_\Gamma}{|\mathbf{b}_\Gamma|}$ are unit vectors and $|\mathbf{a}_\Gamma|$ ($|\mathbf{b}_\Gamma|$) resemble the reciprocal lattice constants in x- and y-direction respectively. The size of a single cluster is given by the number of sites L_x (L_y) in each direction and the real space spanning vectors for the superlattice are given by

$$\mathbf{a}_\Gamma = L_x \hat{\mathbf{x}}, \qquad\qquad \mathbf{b}_\Gamma = L_y \hat{\mathbf{y}} \tag{3.54}$$

Keeping pbc in mind, the coefficients for the reciprocal superlattice wave vectors $\tilde{\mathbf{k}}$ are obtained through

$$\begin{aligned} \tilde{k}_x \;&=\; \frac{2\pi}{|\mathbf{a}_\Gamma| N_x} m_x \;=\; \frac{2\pi}{L_x N_x} m_x, \\ \tilde{k}_y \;&=\; \frac{2\pi}{|\mathbf{b}_\Gamma| N_y} m_y \;=\; \frac{2\pi}{L_y N_y} m_y. \end{aligned} \tag{3.55}$$

The clusters are labeled according to their position $\mathbf{R}_{xy}$ on the two-dimensional lattice, so that m_x runs from 0 to $N_x - 1$ and m_y from 0 to $N_y - 1$. Altogether the crystal momenta $\tilde{\mathbf{k}}$ take on values from 0 to (not including) $\frac{2\pi}{L_x}\hat{\mathbf{x}} + \frac{2\pi}{L_y}\hat{\mathbf{y}}$.

A particular superlattice wave vector in (3.53) reads

$$\tilde{\mathbf{k}} \;=\; 2\pi \sum_\nu \frac{m_\nu}{L_\nu N_\nu} \hat{\nu} \qquad\qquad \nu = x, y \tag{3.56}$$

While hoppings within the clusters are calculated exactly, the inter-cluster hoppings are treated perturbatively.
It is convenient to use matrix notation where $\mathbf{p}$ contains all pseudoparticle excitations belonging to a particular cluster in real space or a certain crystal momentum $\tilde{\mathbf{k}}$ in reciprocal space. The resulting Hamiltonian in mixed representation for the case of a 2x2 cluster tiling has the form

$$\hat{H}(\tau) \;=\; \sum_\sigma \sum_{\tilde{\mathbf{k}}} \; \mathbf{p}^\dagger_{\tilde{\mathbf{k}}}(\tau) \; \mathrm{Q}^\dagger \Big[\mathrm{h}_0 + \mathrm{h}_0^{\mathrm{A}}(\tau) + \mathrm{V}^{\mathrm{A}}(\tau) \Big] \mathrm{Q} \; \mathbf{p}_{\tilde{\mathbf{k}}}(\tau) \tag{3.57}$$

h_0 designates the time independent eigenvalue matrix with elements $\delta_{\alpha\beta}\epsilon_\alpha\eta_\alpha$. The other two terms inside the brackets represent hopping matrices in real space containing the following elements with

regard to our example (the cluster sites have been labeled from left to right and top to bottom in an increasing manner)

$$\mathrm{h}_0^{\mathrm{A}}(\tau) \;=\; \begin{bmatrix} 0 & -te^{-\mathrm{i}\,A(\tau)}-1 & 0 & 0 \\ -te^{\mathrm{i}\,A(\tau)}-1 & 0 & 0 & 0 \\ 0 & 0 & 0 & -te^{-\mathrm{i}\,A(\tau)}-1 \\ 0 & 0 & -te^{\mathrm{i}\,A(\tau)}-1 & 0 \end{bmatrix} \tag{3.58}$$

$$\mathrm{V}^{\mathrm{A}}(\tau) \;=\; \begin{bmatrix} 0 & -te^{-\mathrm{i}(L_x\tilde{k}_x-A(\tau))} & 0 & 0 \\ -te^{\mathrm{i}(L_x\tilde{k}_x-A(\tau))} & 0 & 0 & 0 \\ 0 & 0 & 0 & -te^{-\mathrm{i}(L_x\tilde{k}_x-A(\tau))} \\ 0 & 0 & -te^{\mathrm{i}(L_x\tilde{k}_x-A(\tau))} & 0 \end{bmatrix} \tag{3.59}$$

The three terms, when merged together and transformed by the Q-matrices, produce the full Hamilton matrix $\mathrm{h}_{\tilde{\mathbf{k}}}(\tau)$.
In addition to that we can formally make the time evolution explicit by writing

$$\hat{H}(\tau) \;=\; \sum_{\sigma,\tilde{\mathbf{k}}} \mathbf{p}_{\tilde{\mathbf{k}}}^{\dagger}\mathrm{U}^{\dagger}(\tau)\mathrm{h}_{\tilde{\mathbf{k}}}(\tau)\mathrm{U}(\tau)\mathbf{p}_{\tilde{\mathbf{k}}} \tag{3.60}$$

If the single-particle operators $p_{\gamma,\tilde{\mathbf{k}}}^{\dagger}$ create eigenstates of the Hamiltonian, then the matrix elements directly represent the expectation values corresponding to the system being in one of these states. In any other case an additional unitary transformation can be carried out in order to diagonalize the Hamilton matrix.

3.6 Implementation

Now that the main CPT pseudoparticle formalism for the Hubbard model has been installed, this section gives a few remarks on the computational implementation of the method.
A problem one encounters rather quickly is how to diagonalize the single cluster to arrive at the eigenenergies for $\hat{H}_0$. A major drawback with regard to exact diagonalization (ED) techniques is the fact that the eigenvalue problem grows exponentially with system size and therefore one is restricted to small systems with a maximum of about 16 sites. ED methods are based on the idea that by choosing a suitable basis set the Hamilton matrix can be constructed rather easily and in a following step diagonalized which is especially computer memory expensive.

Impurity solvers on the other hand, which for example use the Lanczos algorithm, can deal with a much larger lattice but are more cumbersome to implement. Furthermore, they are prone to systematic errors and convergence issues because of their approximative nature. Iterative procedures, such as Monte Carlo on the other hand, are less memory intensive but very time expensive.

With respect to the representation of the basis set, a very useful and convenient coding scheme for the cluster basis is the following: Specify the basis states by the occupation number (0 or 1) of electrons at each site, where the occupation numbers of spin up electrons are to the left of the spin

down numbers. The obtained series of strings specifies unambiguously the occupation pattern and constitutes a binary representation of any given state.
Consider for example a 4-site cluster with its symbolical representation of spin up and spin down electrons leading to a unique binary delineation

$$|\downarrow, 0, \uparrow\downarrow, \uparrow\rangle \;=\; c^{\dagger}_{3\uparrow} c^{\dagger}_{4\uparrow} c^{\dagger}_{1\downarrow} c^{\dagger}_{3\downarrow} \,|0\rangle \quad\rightarrow\quad 00111010 \tag{3.61}$$

As already mentioned in Sec. 2.2.2, the order in which the creation operators appear is a matter of convention but has to be obeyed thoroughly. Therefore, an integer can be assigned unambiguously to every state, making the storage of all basis states quite efficient. The assigned integer can be decomposed into a spin up and a spin down part

$$\mathrm{int} \;=\; \mathrm{int}_{\downarrow} + 2^{L}\, \mathrm{int}_{\uparrow} \tag{3.62}$$

yielding $58{=}10{+}2^4{\cdot}3$ in the example above. This can be further decomposed to recover the original occupation number for each cluster site.

The degrees of freedom or the number of basis states in general and thereby the dimensionality of the full Hilbert space is 4^L. For a given value of $\mathbf{S}^z$ this becomes $\binom{L}{N_\uparrow}\binom{L}{N_\downarrow}$, which is maximal for a half-filled zero-spin system. The ground state belongs to the sector of the Hilbert space where $N_\uparrow = N_\downarrow$. Accordingly, this measures up to a total number $\binom{L}{L/2}^2$ of basis states, which behaves like $4^L/L$ for large clusters.
As an example, in the case of a 4-site cluster the full Hilbert space consists of 265 states, whereas the Fock basis for a half-filled system contains only 36 states. However, the pseudoparticle basis of single-particle excitations that essentially determines the size of the Hamilton matrix for a particular spin σ and crystal momentum $\tilde{\mathbf{k}}$ is always larger than the Fock basis, except in the case of $L = 2$ where both basis sets are of the same size.

The real space matrix elements are constructed by summing up all non-zero contributions from each spin and site in the Hubbard Hamiltonian. The interaction strength U enters exclusively on the main diagonal since correlations between two particles occur only on the same site. The off-diagonal matrix elements arise from hopping processes with potentially an additional sign resulting from Fermi statistics.

Chapter 4

Current density

The bridge between simulations and experiments are observables, i. e. quantities that can be measured in experimental setups and are represented by expectation values of the corresponding quantum mechanical operators. This chapter is devoted to calculating the expectation value of the current density operator which itself is derived from the CPT-Hamiltonian.

In its very general form the Hamiltonian consists of a part related to the kinetic energy ($\hat{K}$) and an interaction term originating from the Coulomb potential

$$\hat{H} \;=\; \hat{K} + \hat{H}_{int} \tag{4.1}$$

The electric current accounts for the moving of particles through the crystal lattice, so only the kinetic term directly contributes. In its full embodiment $\hat{K}$ is given by

$$\hat{K} \;=\; \sum_{\sigma} \sum_{i,j} t_{ij} c^{\dagger}_{i,\sigma} c_{j,\sigma} \tag{4.2}$$

As we are considering only nearest-neighbor hopping, the matrix elements are reduced to $t_{ij} = -t$ for $|\mathbf{R}_i - \mathbf{R}_j| = 1$ (in units of the lattice constant) and $t_{ij} = 0$ otherwise. In order to increase readability the spin index is omitted in the following because it only enters as a parameter.

Introducing the electrical field through Peirls' substitution yields

$$\hat{K}(\tau) \;=\; -t \sum_{\sigma} \sum_{\langle i,j \rangle} e^{\mathrm{i}\,\mathbf{A}(\mathbf{R}_i - \mathbf{R}_j)}\; c^{\dagger}_i c_j \tag{4.3}$$

The current density operator has the form [43]

$$\hat{J} \;=\; -\frac{\partial}{\partial \mathbf{A}} \hat{K}(\tau) \tag{4.4}$$

In the case of the one-dimensional chain, after performing a standard Fourier transformation and a short manipulation, this results in the expression

$$\hat{J}^{(1\mathrm{D})} \;=\; -2t \sum_{\sigma} \sum_{k} \sin(k + A) c^{\dagger}_k c_k \tag{4.5}$$

Linear response limit

Briefly and in parenthesis the current density in the context of a weak external perturbation, that is a small electric field, shall be mentioned here (cf. Refs. [12, 43]).
In the linear response limit the expression (4.3) for the kinetics of the system can be approximated by a Taylor series expansion around $A = 0$. Without writing the time dependence explicitly the expansion up to second order gives

$$\hat{K}_A \;=\; \sum_{\sigma} \sum_{\langle i,j \rangle} \left(-t \;-\; \mathrm{i}\, At \;+ \frac{A^2}{2} t \right) c_i^\dagger c_j \;+\; \text{h.c.} \tag{4.6}$$

Thus, the current density operator takes on the form

$$\hat{J} \;=\; \sum_{\sigma} \sum_{\langle i,j \rangle} (\mathrm{i}\, t - At)\, c_i^\dagger c_j \;+\; \text{h.c.} \tag{4.7}$$

and a Fourier transformation for the atomic chain in 1D would amount to

$$\hat{J}^{(1\mathrm{D})} \;=\; -2t \sum_{\sigma} \sum_{k} \Big(\sin k + A \cos k \Big)\; c_k^\dagger c_k \tag{4.8}$$

However, for large electric fields this is no longer valid and we stick to the general expression of the kinetic part of the Hamiltonian.

4.1 CPT expression for the current density

The cluster tiling breaks translational symmetry on the lattice and it is no longer possible to perform a full Fourier transformation directly. We rename the creation and annihilation operators according to the cluster they belong to, such that $c_i \equiv c_{n,a}$ where a stands for the cluster index and n denotes the site inside the cluster.

The overall current consists of an intra-cluster as well as an inter-cluster part, $\hat{J} = \hat{J}_0 + \hat{J}'$, and has the form

$$\hat{J} = -t \sum_{\sigma} \sum_{a,b} \sum_{\langle n,m \rangle_x} \mathrm{i}\, e^{-\mathrm{i}\, A} c_{n,a}^\dagger c_{m,b} \Big(\delta_{a,b} + \delta_{a+1,b} \Big) \tag{4.9}$$

The shortened notation with a sum over $\langle n, m \rangle_x$ indicates that only neighboring sites n, m where $|\mathbf{R}_\mathbf{x}(n) - \mathbf{R}_\mathbf{x}(m)| = 1$ are considered. The restriction to sites along the x-direction is due to the electric field being chosen parallel to $\mathbf{x}$ which means that there is no current flowing perpendicular to it in y-direction.
The first Dirac δ-function accounts for the intra-cluster current and the second one pays tribute to the current that is arising from hoppings across cluster boundaries.

In two dimensions and in mixed representation one obtains

$$\hat{J} \;=\; -t \sum_{\sigma} \sum_{\tilde{\mathbf{k}}} \left[\sum_{\langle n,m \rangle_x} \mathrm{i}\, e^{-\mathrm{i}\, A} c_{n,\tilde{\mathbf{k}}}^\dagger c_{m,\tilde{\mathbf{k}}} \;-\; \sum_{\langle n',m' \rangle_x} \mathrm{i}\, e^{-\mathrm{i}(\tilde{k}_x L_x - A)} c_{n',\tilde{\mathbf{k}}}^\dagger c_{m',\tilde{\mathbf{k}}} \right] \tag{4.10}$$

The second sum with primed indices n', m' runs over neighboring sites along the cluster boundaries and represents the inter-cluster contribution to the current.

In the next step we transform the operators according to $c_{n,a} = \sum \mathrm{Q}_{n\alpha} p_{\alpha,a}$ which projects the cluster sites onto the pseudoparticle excitations.
In matrix notation (with Einstein's sum rule implied) this may be rewritten as

$$\hat{J}(\tau) \;=\; \sum_{\sigma} \sum_{\tilde{\mathbf{k}}} \Big[p^{\dagger}_{\alpha,\tilde{\mathbf{k}}} \mathrm{Q}^{\dagger}_{\alpha n} \mathrm{C}_{nm,\tilde{\mathbf{k}}} \mathrm{Q}_{m\beta} p_{\beta,\tilde{\mathbf{k}}} \Big]_{\tau} \tag{4.11}$$

where the expression inside the parentheses is evaluated at time τ.

To give an example, in the case of a linear 4-site cluster the hopping matrix has the form

$$\mathrm{C}^{(1\mathrm{x}4)}_{\tilde{k}} \;=\; -t \begin{bmatrix} 0 & \mathrm{i}\, e^{-\mathrm{i}\, A} & 0 & -\mathrm{i}\, e^{-\mathrm{i}(\tilde{k}L - A)} \\ -\mathrm{i}\, e^{\mathrm{i}\, A} & 0 & \mathrm{i}\, e^{-\mathrm{i}\, A} & 0 \\ 0 & -\mathrm{i}\, e^{\mathrm{i}\, A} & 0 & \mathrm{i}\, e^{-\mathrm{i}\, A} \\ \mathrm{i}\, e^{\mathrm{i}(\tilde{k}L - A)} & 0 & -\mathrm{i}\, e^{\mathrm{i}\, A} & 0 \end{bmatrix} \tag{4.12}$$

Note, there is no difference in the expression for the current whether the lattice consists of a one-dimensional chain or linear clusters in 2D that are only connected perturbatively in the direction perpendicular to the electric field.

For quadratic 4-site clusters the matrix elements are given by, cf. equations (3.58) and (3.59),

$$\mathrm{C}^{(2\mathrm{x}2)}_{\tilde{\mathbf{k}}} \;=\; \begin{bmatrix} 0 & \xi & 0 & 0 \\ \xi^{*} & 0 & 0 & 0 \\ 0 & 0 & 0 & \xi \\ 0 & 0 & \xi^{*} & 0 \end{bmatrix} \tag{4.13}$$

where $\xi = -\mathrm{i}\, t \left(e^{-\mathrm{i}\, A} - e^{-\mathrm{i}(\tilde{k}_x L_x - A)} \right)$ and ξ^{*} symbolizes its complex conjugate.
The sign for the vector potential in the two exponentials differs because the first term describes intra-cluster hoppings where the site index increases from left to right, thus giving a minus sign for the Peierls phase for hoppings to the left (i.e. along the positive x-direction), and the second term describes inter-cluster hoppings for which the site index decreases from left (last site of one cluster) to the right (first site of the second cluster).
The phase factor $\exp(-\mathrm{i}\, \tilde{k}_x L_x)$ originates from the superlattice Fourier transformation and takes into account the extension L_x of the cluster in the direction of the electric field.
By analogy and taking into account considerations with respect to particular lattice tilings this can be extended to clusters of any size or shape.

4.2 Expectation values

The CPT expression for the current (4.11) needs some additional manipulations in order to arrive at an expectation value for the time dependent current density $\langle \hat{J}(\tau) \rangle$.
We are interested in expectation values of the kind $\langle p^{\dagger}_{\gamma}(\tau) p_{\gamma'}(\tau) \rangle$ where γ stands for a compound index including all quantum numbers, such as momentum, site and spin. The time dependence of

the operators can be extracted as we have seen in Sec. 3.4. Pulling all time dependence in front of the operators, and thereby outside the estimator, leaves us with an expression that is proportional to $\langle p^\dagger_\gamma p_{\gamma'} \rangle_{\tau=0}$.

The pseudoparticle operators $p^\dagger$ (p) create (annihilate) eigenstates of the single cluster Hamiltonian $\hat{H}_0$. However, the total Hamiltonian $\hat{H}(\tau) = \hat{H}_0 + \hat{V}(\tau)$ is not diagonal in this basis set.
For times before and including $\tau = 0$ the system is in its ground state because it is still unperturbed and in equilibrium. Hence, we perform an additional diagonalization of the lattice Hamiltonian at $\tau = 0$ by means of ED. The operators in the new eigenbasis are labeled $f^\dagger_\gamma$ and $f_{\gamma'}$ to distinguish them from the original ones of the cluster basis. The transformation of the Hamilton matrix and the operators may be written as

$$\mathrm{h}(\tau = 0) \;\longrightarrow\; \mathrm{W}^{-1}\mathrm{h}(\tau = 0)\mathrm{W} \qquad \{\mathbf{p}, \mathbf{p}^\dagger\}_{\tau=0} \;\longrightarrow\; \{\mathbf{f}, \mathbf{f}^\dagger\} \tag{4.14}$$

The new operators diagonalize the total Hamiltonian in equilibrium and, since the time dependence has already been dealt with, they are also independent of time.

The electrons as well as the pseudoparticle excitations obey Fermi statistics. With regard to the full lattice the particle distribution in the ground state is governed by Fermi's distribution function, which at zero temperature turns into Heaviside's step function

$$f_F(\epsilon, T) \;=\; \frac{1}{e^{(\epsilon-\mu)/k_B T} + 1} \;\overset{T\to 0}{=}\; \Theta(\mu - \epsilon) \tag{4.15}$$

The eigenvalues of the lattice Hamiltonian that have been computed through the diagonalization process (4.14) enter into the distribution function and thereby the ground state of the system is attained.

The eigenstates of the CPT Hamiltonian form an orthonormal basis set, which means that all but the diagonal elements of the estimator are vanishing. Only operators acting on the same states contribute, i.e. $\delta_{\gamma\gamma'}\langle f^\dagger_\gamma f_{\gamma'}\rangle_{\tau=0} = f_F(\epsilon_\gamma)$, where ϵ_γ denote the eigenenergies of the equilibrium Hamiltonian such that $\hat{H}|\gamma\rangle = \epsilon_\gamma|\gamma\rangle$.

To conclude the considerations so far, the expectation value of the current for a given set of quantum numbers may be expressed as

$$\left\langle \hat{J}(\tau) \right\rangle_\gamma \;\propto\; \mathrm{D}[\hat{U}(\tau), A(\tau)] \left\langle f^\dagger_\gamma f_\gamma \right\rangle \tag{4.16}$$

with some functional $\mathrm{D}[U(\tau), A(\tau)]$ depending on the vector potential and the time evolution of the operators.

Generally we are interested in the case of half-filling where the chemical potential is equal to $\mu = U/2$ due to particle-hole symmetry. This means for the expectation value that $\langle f^\dagger_\gamma f_\gamma \rangle = \Theta(\frac{U}{2} - \epsilon_\gamma)$.

Finally, the current density per lattice site is simply given by

$$j(\tau) \;=\; \frac{1}{\Lambda}\left\langle \hat{J}(\tau) \right\rangle \tag{4.17}$$

In summary, the CPT-expression for the current density in matrix notation has the form

$$j(\tau) \;=\; \frac{1}{\Lambda} \sum_\sigma \sum_{\tilde{\mathbf{k}}} \left[\mathrm{W}^\dagger \mathrm{U}^\dagger(\tau) \mathrm{Q}^\dagger \mathrm{C}(\tau) \mathrm{Q} \mathrm{U}(\tau) \mathrm{W} \left\langle \mathbf{f}^\dagger \mathbf{f} \right\rangle \right]_{\tilde{\mathbf{k}},\sigma} \tag{4.18}$$

4.3 Limiting cases

The level of abstraction or approximation in any CPT procedure is determined by the size of the clusters. The results obtained from CPT calculations become more accurate with an increasing amount of sites inside the clusters, leading to the exact outcome in the limit of an infinitely large cluster ($L \to \infty$). This is evidently true since the clusters are solved exactly and an infinitely large cluster would encompass the whole lattice.
Apart from this there are two other limits where CPT is capable of delivering the exact answer: the noninteracting as well as the atomic limit.

4.3.1 Noninteracting limit

In the case of free particles ($U = 0$) the one- or two-dimensional Hubbard model can be solved analytically. When there is no interaction present the lattice Hamiltonian

$$\hat{H} \;=\; -t \sum_{\langle i,j\rangle,\sigma} (c^{\dagger}_{i\sigma} c_{j\sigma} + c^{\dagger}_{j\sigma} c_{i\sigma}) \tag{4.19}$$

consists only of one-particle terms and can, at least in principle, readily be diagonalized by ordinary Fourier transformation

$$c^{\dagger}_{i\sigma} \;=\; \frac{1}{\sqrt{\Lambda}} \sum_{\mathbf{k}} e^{\mathrm{i}\,\mathbf{k}\mathbf{R}_i}\; c^{\dagger}_{\mathbf{k}\sigma} \tag{4.20}$$

The system's Hamiltonian is translational invariant and periodic boundary conditions are assumed. The transformation directly yields the eigenenergies which are given by the dispersion relation (depending on the dimensionality d of the problem and with $\mathbf{a}$ the lattice constant)

$$\epsilon_{\mathbf{k}} \;=\; -2t \sum_{d} \cos(\mathbf{k}_d \mathbf{a}) - \mu \tag{4.21}$$

The diagonalized noninteracting Hamiltonian then has the form

$$\hat{H}^{\mathrm{U}=0} \;=\; \sum_{\mathbf{k},\sigma} \epsilon_{\mathbf{k}} c^{\dagger}_{\mathbf{k}\sigma} c_{\mathbf{k}\sigma} \tag{4.22}$$

By leaving out the electron-electron correlations altogether the nearest neighbor tight-binding solution for free fermions is recovered and the orbitals may be written in the form of plane waves $\phi_{\mathbf{k}} = \frac{1}{\sqrt{\Lambda}} e^{\mathrm{i}\,\mathbf{k}\mathbf{r}}$ which are eigenstates of the momentum operator with definite wave numbers $|\mathbf{k}|$.

The ground state of the system is obtained by filling the energy levels up to the Fermi level ($\mu = \epsilon_F$ at temperature $T = 0$).
At half-filling each $\mathbf{k}$-state can be occupied by two electrons of either spin. Without having to pay a penalty U for double occupancy, the lower half of the energy spectrum up to the Fermi edge is doubly occupied while the other half is completely empty.

Thus, the ground state in the noninteracting limit is given by the Fermi sea,

$$|GS\rangle = \prod_{\mathbf{k}\leq\mathbf{k_F}} c^{\dagger}_{\mathbf{k}\uparrow} c^{\dagger}_{\mathbf{k}\downarrow} |0\rangle \tag{4.23}$$

Note that at finite temperatures the ground state would be given by a sum over all eigenstates weighted by the associated Boltzmann factor.

For large interaction strengths the system exhibits insulating behavior but when U approaches zero it becomes more and more metallic. In the limit of $U = 0$ it can be thought of as a perfect metal in the sense that the system's conductivity is optimal because the electron's motion through the lattice is unimpeded by its fellow particles.

In terms of CPT, the noninteracting limit means that instead of diagonalizing the single cluster to determine the excitation energies, we can directly access the eigenvalues by writing the Hamiltonian in its eigenbasis of plane wave functions.

The full Fourier transformation of (4.3) has the form

$$\hat{K}(\tau) \;=\; -2t \sum_{\sigma} \sum_{\mathbf{k}} \left[\cos\left(k_x + A(\tau)\right) + \cos(k_y)\right] \; c^{\dagger}_{\mathbf{k}}(\tau) c_{\mathbf{k}}(\tau) \tag{4.24}$$

and the expression for the current is readily obtained as

$$\hat{J}(\tau) = \; -2t \sum_{\sigma} \sum_{\mathbf{k}} \sin\left(k_x + A(\tau)\right) \; c^{\dagger}_{\mathbf{k}}(\tau) c_{\mathbf{k}}(\tau) \tag{4.25}$$

The expectation value of which is given by

$$\left\langle \hat{J}(\tau) \right\rangle \;=\; -2t \sum_{\sigma} \sum_{\mathbf{k}} \sin\left(k_x + A(\tau)\right) \; \left\langle c^{\dagger}_{\mathbf{k}} c_{\mathbf{k}} \right\rangle_{\tau=0} \tag{4.26}$$

At time $\tau = 0$ before the electric field is turned on, the system is in the ground state. And by expressing the estimator in terms of Fermi's distribution function we arrive at the analytical result

$$j(\tau)^{\mathrm{U}=0} \;=\; -\frac{2t}{\Lambda} \sum_{\sigma} \sum_{\mathbf{k}} \sin\Big(k_x + A(\tau)\Big) \; f_F\Big(-2t[\cos k_x + \cos k_y] - \mu\Big) \tag{4.27}$$

In the case of linear clusters the current density per site does not depend on the dimensionality of the lattice (1D or semi-2D), whereas the amplitude changes when considering a truly two-dimensional cluster tiling.

4.3.2 Atomic limit

In the strong coupling or atomic limit ($t/U \to 0$) CPT also arrives at the exact result. By setting $t = 0$ (or equivalently $U = \infty$) any particle mobility is disabled. The electrons are confined to staying at their parent lattice ions and consequently the model exhibits insulating behavior because no conducting states are possible.
Charge fluctuations are completely frozen out (or suppressed) leading to a perfect Mott insulator [21] and double occupancy is diminishing proportional to t/U^2 as U goes to infinity.

In the atomic limit the Hubbard model maps onto the Heisenberg model which has an antiferromagnetic ground state. The original Hubbard model on the other hand leaves magnetic ordering out of the picture.

The ground state at half-filling is highly degenerate since each site is occupied by one electron with arbitrary spin orientation.

The system's Hamiltonian is reduced to its interaction part only since no hopping processes are allowed for. $\hat{H}_{int}$ is already diagonal, considering merely on-site interactions, and the electrons can be thought of as behaving more like 'particles' in contrast to a more 'wave-like' behavior in the noninteracting case.

4.4 Mott insulator

Certain materials are expected from conventional band theory calculations considering delocalized electrons to behave like conductors because they have an odd number of electrons per unit cell. However, in experiments it turned out that some of them are in fact insulators. This somewhat puzzling behavior can be attributed to the partially freezing out of charge fluctuations [21].
Materials with such characteristics are named Mott insulators and so called Mott or metal-insulator transitions (MIT) from insulating to conducting phases are predominantly observed in transition metal compounds with partially filled bands near the Fermi level.
For example $SrCuO_2$ and Sr_2CuO_3 as well as V_2O_3 doped with Cr are found to demonstrate Mott insulating behavior. In addition to that, carbon nanotubes have been predicted - and to some extend experimentally confirmed - to realize 1D Mott insulators [44].

Very recently the formation of a Mott insulator of a repulsively interacting two-component Fermi gas was experimentally realized for the first time [6]. The group observed most notably a strong suppression of double occupancy and the appearance of a gapped mode in the excitation spectrum of the system.

On the theoretical side, the band structure description provides a good insight into the properties of ionic insulators, ordinary semiconductors or simple metals by considering filled and empty bands or, in the case of metals, at least one partially filled band and disregarding any particle interactions. The Hubbard model, as opposed to band theory, does take into account electron-electron correlations which play a crucial role in the formation of an energy gap within the band structure when the interaction U is sufficiently large. The excitation gap in a Mott insulator is qualitatively very different from the band gap in a conventional band insulator because it originates directly from the electron-electron repulsion. Band insulators on the other hand have fully filled or completely empty bands that are separated by an energy gap in the density of states.
Every phase transition has an ordering parameter and for the MIT it is expected to be U. The MIT is supposed to occur somewhere in the range where U is of the same order as t, i.e. $U_c \sim t$.
If we consider large overlap integrals, the energy bands are broadening and at some point when t becomes large enough with respect to U the bands merge again, thus forming a insulator-metal transition.

When there is no external field applied to the system, the ground state of the 1D Hubbard model is a Mott insulator for all $U > 0$. There is no conducting-insulating transition in the ground state except in the case of no interaction where U is exactly equal to zero [22].
In the 2D Hubbard model a Mott transition occurs at some critical value $U_c > 0$ and the opening gap is enlarged with increasing U.

In the case of the FK model at half-filling, the Mott transition was determined to occur at $U_c = \sqrt{2}$ in the infinite-dimensional limit (cf. Ref. [45]).

With a strong electric field present the system starts to exhibit quantum tunneling from the ground state to excited states [46] and phenomena like a dielectric breakdown of the insulator can be observed. Applying a large external field drives the system out of equilibrium and essentially destroys the Mott insulating state. For band insulators it is more or less well understood how a dielectric breakdown happens through the effects of Zener tunneling. But it is not clear yet if the same explanations can be applied to Mott insulators as well.

According to recent investigations of a one-dimensional Hubbard chain attached to noninteracting leads where a bias voltage is applied, the dielectric breakdown of the 1D Hubbard model can be understood in terms of Zener tunneling in the same way as in the case of a band insulator if one exchanges the band gap with the Mott gap [47]. On the other hand, also in a recent publication, the authors state that it is not clear from their (t-DMRG) calculations whether the Landau-Zener mechanism applies when the system is not coupled to leads [48].
For details on the ongoing discussion see the above mentioned references and references therein.

Another area of interest with regard to Mott insulators is the fact that some Mott insulators undergo a transition from insulating to superconducting behavior when weakly doped with additional charge carriers. It is assumed (see for example Ref. [49]) that by understanding the transitional phases the formation of high-T_c superconductors, which so far remains a mystery of modern physics, can finally be explained.

4.5 Bloch oscillations

The investigation of expectation values for the current density leads to the prominent phenomenon of Bloch oscillations that occur in the time resolved pattern of the electric current.
Bloch oscillations describe the movement of particles in a periodic potential when a constant external force is applied. In our case the particles are electrons (or holes) moving in a crystal while exposed to a spatially uniform electric field pointing in a direction parallel to a lattice vector.
The electric force $\mathbf{F} = e\mathbf{E}$ is given by Coulomb's law, with the elementary charge e and the electric field strength being either constant, $\mathbf{E} = E_0\mathbf{x}$, or oscillating in time, $\mathbf{E}' = [E_0 + E_1 \cos(\omega\tau)]\,\mathbf{x}$.

The occurrence of oscillations is somewhat counterintuitive and classically one would expect a strictly ohmic behavior. If the same electrons were flowing through space under the influence of the same voltage they would simply accelerate and gain energy in a uniform manner. However, the additional presence of a regular pattern due to a spatially varying potential that is created by atoms of the crystal lattice leads to some interesting phenomena.

There are certain energy values that an electron cannot occupy because of resonance with the lattice. These forbidden energies lie within the electronic band gaps. As the energy of an accelerating electron approaches the gap edge, it is strongly back scattered by the lattice. Such acceleration and back scattering processes cause electrons to wobble back and forth in space, producing the oscillatory effect named after F. Bloch.

The phenomenon was first described by Bloch [15] in the late 1920s and was elaborated on a few years later by Zener [50]. Where classical mechanics fails to give an explanation, quantum mechanics predicts that the particles will undergo an oscillation due to the fact that the periodicity of the lattice potential causes the group velocity of the wave function to oscillate.

One of the early experimental confirmations of Bloch oscillations was carried out by measuring the optical dephasing of Wannier-Stark ladder excitations in a semiconductor superlattice [51].
Within the last two decades Bloch oscillations have been observed in semiconducting heterostructures [52], Josephson junctions [53] and ultracold atoms trapped in optical lattices [54].
In addition, Bloch oscillations can also serve as a source for dipole radiation in the terahertz range (see e.g. Ref. [55] and references therein).
However, up to now Bloch oscillations have never been observed in metals or Mott insulators because of the very short electron relaxation time. The electrons are scattering at impurities within the crystal before they are able to reach the Brillouin zone boundary.

The most recent experimental realizations predominantly use ultracold atoms placed in an optical lattice [56]. By detuning the lasers it appears as if the optical lattice would produce a standing wave in a moving frame, which is equivalent to the lattice being 'pulled through' the atomic system.
This in turn resembles the Hamiltonian gauge $\Phi(\mathbf{r}, \tau) = 0$ that we are using numerically in our CPT calculations. Although it is not possible to measure the current directly in these experiments, it can be reconstructed from time of flight measurements.

In Fig. 4.1 two experiments using Bose-Einstein condensates (BEC) in optical lattices are displayed. In panel (a) a time of flight measurement is shown and panel (b) portrays the spatial density of a BEC under the influence of bichromatic laser beams that are forming the lattice potential.

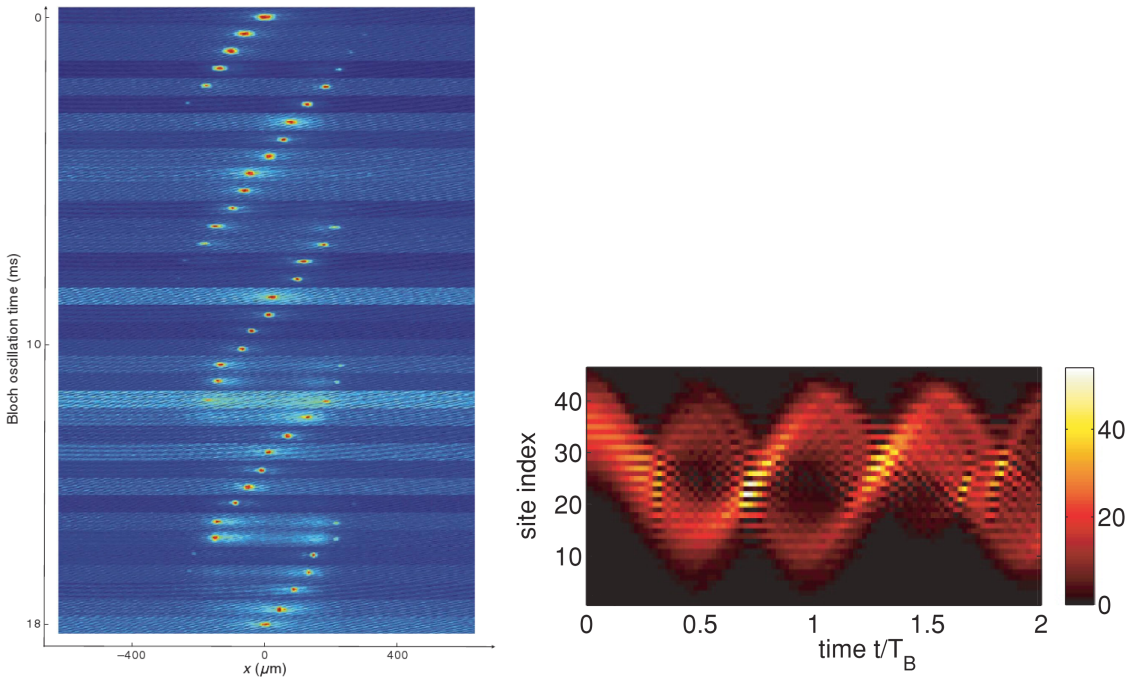

(a) (b)

Figure 4.1: (a) Absorption images after a time of flight of 30ms, for varying Bloch oscillation times and an acceleration of $2.4 m/s^2$ [57], (b) Bloch oscillations of a BEC of 300 atoms in a tilted bichromatic lattice, shown is the atomic density in real space [58].

All these experiments concerning cold atoms are dealing with Bosons. So far it was not possible to reach the very strong temperature requirements which would be necessary to fully realize trapped fermions in an optical lattice. However, experimentalists are optimistic to achieve the required

conditions within a couple of years.

Considering a constant external field, Bloch oscillations occur with a period $T_B = \frac{h}{eE_0 a}$ or rather in atomic units and with lattice constant a set to one

$$T_B = \frac{2\pi}{E_0} \tag{4.28}$$

In the case of a alternating electric field and no constant contribution, i.e. $E_0 = 0$, the Bloch oscillations are driven by the field's frequency ω and the Bloch period becomes

$$T'_B = \frac{2\pi}{\omega} \tag{4.29}$$

A detailed discussion of the numerical results featuring Bloch oscillations is given in chapter 5.

As an example Fig. 4.2 shows Bloch oscillations for small interaction strengths at $E_0 = 1$. The result for $U = 0$ was calculated analytically and serves as reference for the numerical data.
In the case of zero on-site interaction (i.e. no scattering from electrons with opposite spin), the Bloch oscillations are perfectly harmonic functions extending infinitely in time. When the interaction is turned on ($U > 0$) the oscillations at first maintain their periodicity, at least for small values of U. As the correlations increase the oscillations become more and more irregular, as can be seen for example in the case of $U = 1$ (cyan line). There is also a U-dependent damping of the amplitude visible that becomes dominant for larger interaction strengths.

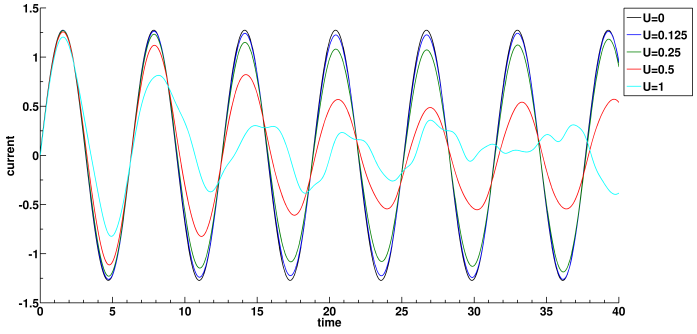

Figure 4.2: Non-equilibrium current for different values of U at $E_0 = 1$ for a half-filled 1D chain of 4-site clusters (time step $d\tau = 0.03$, number of clusters $N_c = 20$).

Chapter 5

Numerical calculations

In this chapter we present results from CPT calculations of the non-equilibrium current as a function of time under several conditions, including different cluster sizes and shapes, half-filling, band doping, static as well as oscillating electrical fields. As far as available we also try to build a bridge to recent results obtained by DMFT and t-DMRG techniques.

Throughout this chapter the results are expressed in terms of the parameters that are used. Thus, energies are given in units of the hopping strength t which, for example, corresponds to about 0.5eV in the case of high-temperature superconducting compounds. The time τ is given in units of $\hbar/t$. As we are considering time frames of up to $\tau \approx 100$ at most, this means that we are dealing with time windows of the order of a few hundred femtoseconds up to the order of picoseconds.
The period of Bloch oscillation lies in the range of $10-100$ femtoseconds which amounts to a typical Bloch frequency in the terahertz region. The electric field is formulated in terms of hopping t and the lattice constant. Considering characteristic lattice spacings of a few Å leads to a corresponding electric field of the order of several mV/Å.

Analytical investigations

As already mentioned before in Sec. 4.3, CPT becomes exact in the noninteracting limit where $U = 0$. In this case the current density can be calculated analytically, which comes in handy as a useful test and a reference frame for further numerical calculations.

The expression for the current density is given by (4.26). For a static external electric field the vector potential is linear in time, $A(\tau) = E_0\tau$. By inserting this in (4.26) the oscillatory behavior of the current density becomes evident. The frequency of which is proportional to the strength of the electric field and the Bloch period can be expressed as given in (4.28).

An additional check can be carried out by calculating the expectation value of the particle number operator which in the case of half-filling is equal to the total number of lattice sites, i.e. $\langle \hat{N} \rangle \stackrel{!}{=} \Lambda$. The numerical computation is sketched in matrix notation as follows

$$\hat{N} \;=\; \sum_i (n_{i\uparrow} + n_{i\downarrow}) \;=\; \sum_{i,\sigma} c^\dagger_{i,\sigma} c_{i,\sigma}$$

$$\hat{N} \;=\; \sum_{a,\sigma} \mathbf{p}^\dagger_a(\tau)\; Q^\dagger Q\; \mathbf{p}_a(\tau) \;=\; \sum_{\tilde{\mathbf{k}},\sigma} \mathbf{p}^\dagger_{\tilde{\mathbf{k}}}(\tau)\; Q^\dagger Q\; \mathbf{p}_{\tilde{\mathbf{k}}}(\tau)$$

$$\hat{N} \;=\; \sum_{\tilde{\mathbf{k}},\sigma} \mathbf{p}^{\dagger}_{\tilde{\mathbf{k}}}(0)\; U^{\dagger}(\tau)Q^{\dagger}QU(\tau)\; \mathbf{p}_{\tilde{\mathbf{k}}}(0) \;=\; \sum_{\tilde{\mathbf{k}},\sigma} \mathbf{f}^{\dagger}_{\tilde{\mathbf{k}}}\; W^{\dagger}U^{\dagger}(\tau)Q^{\dagger}QU(\tau)W\; \mathbf{f}_{\tilde{\mathbf{k}}}$$

$$\langle \hat{N} \rangle \;=\; \sum_{\tilde{\mathbf{k}},\sigma} \Big[W^{\dagger}U^{\dagger}(\tau)Q^{\dagger}QU(\tau)W\; \Theta\big(\mu - D[\epsilon]\big) \Big]_{\tilde{\mathbf{k}},\sigma} \tag{5.1}$$

where the argument of the Theta-function in the last line is the diagonal matrix of the single cluster eigenenergies.

5.1 Staggered on-site potential

As an intermediate approach between the analytically solvable noninteracting model on the one hand and the numerically obtained CPT results on the other, we introduce a staggered on-site potential instead of the interaction U. This is a possible way to simulate a genuine band insulator, in contrast to the Mott insulating behavior of the Hubbard model.
A potential $\Delta/2$ with alternating sign between adjacent atomic sites leads to the development of two distinct bands separated by an energy gap of size Δ. The corresponding Hamiltonian (also known as the ionic Hubbard model [59]) in 1D is given by

$$\hat{H} \;=\; -t \sum_{\langle i,j\rangle,\sigma} (c^{\dagger}_{i,\sigma}c_{j,\sigma} \;+\; c^{\dagger}_{j,\sigma}c_{i,\sigma}) + \frac{\Delta}{2}\sum_{i,\sigma}(-1)^i\; n_i \tag{5.2}$$

Due to the spatially alternating field the unit cell of the underlying lattice now includes two lattice sites with an attractive and repulsive on-site potential respectively.

After including the Peierls phase factor for the external electric field, a Fourier transformation leads to the symmetric expression

$$\hat{H}(\tau) \;=\; \sum_{\sigma}\sum_{k} \begin{pmatrix} c_k \\ c_{k+Q} \end{pmatrix}^{\dagger} \begin{bmatrix} -2t\cos(k+A(\tau)) & \frac{\Delta}{2} \\ \frac{\Delta}{2} & 2t\cos(k+A(\tau)) \end{bmatrix} \begin{pmatrix} c_k \\ c_{k+Q} \end{pmatrix} \tag{5.3}$$

where $Q = \pi$ is a vector of the reciprocal superlattice and the sum runs over crystal momenta k inside the reduced antiferromagnetic Brillouin zone. The diagonal of the Hamiltonian consists of ordinary one-dimensional dispersion relations for free particles, $\epsilon_k = -2t\cos(k + A(\tau))$. For the lower element on the diagonal we took advantage of the fact that $\epsilon_{k+Q} = -\epsilon_k$.

The Hamiltonian is diagonalized at time $\tau = 0$ by introducing new creation and annihilation operators $\gamma^{i\dagger}$ and γ^i with $i = \{1, 2\}$ such that [60]

$$\begin{aligned} \gamma^1_k &= u_k c_k + v_k c_{k+Q} \\ \gamma^2_k &= u_k c_k - v_k c_{k+Q} \end{aligned} \tag{5.4}$$

where $u_k = \sqrt{\frac{1}{2}(1+\epsilon_k/E_k)}$ and $v_k = \sqrt{\frac{1}{2}(1-\epsilon_k/E_k)}$. The energies $E_k = \sqrt{4t^2\cos^2(k) + \Delta^2/4}$ represent the eigenvalues of the diagonalized Hamiltonian.

Differentiating the Hamilton operator with regard to the vector potential yields the familiar relation for the current density

$$\hat{J}(\tau) \;=\; \sum_{\sigma} \sum_{k} \gamma_k^{\dagger}(\tau)\ \mathrm{C}\ \gamma_k(\tau) \tag{5.5}$$

with elements $\pm 2t \sin(k + A(\tau))$ on the main diagonal of the coefficient matrix C and vector operators such that $\gamma_k = (\gamma_k^1, \gamma_k^2)^T$.

The operators γ_k are still time dependent and therefore a unitary transformation according to the time evolution scheme in Sec. 3.4 is carried out. The expectation values are again obtained from Fermi's distribution function $f_F(E_k)$, resulting in the end in an expression for the current density similar to that in (4.18).

In the limit of $\Delta = 0$ the above expression recovers the original noninteracting result as given in (4.26).
For $\Delta > 0$ the energy spectrum splits into two distinct bands that are separated by a gap of size Δ. The ionic Hubbard model thus describes a band insulator which allows us to compare some of the results with those gathered from the Mott insulating Hubbard model. In order to do so the bandgap Δ has to be adjusted to the Mott gap that is opening up for different interaction strengths.
For example, the 1D Hubbard model with $U = 4$ has a Mott gap of about $\Delta_{\mathrm{gap}} = 2.66$. By setting $\Delta = \Delta_{\mathrm{gap}}$ we can construct both a band insulator and a Mott insulator with equal energy gaps.

5.2 Cluster shapes, sizes and dimensions

Starting from the simplest cluster, i.e. one consisting of 2 sites on a one-dimensional lattice, we move upwards to more complex structures in semi-2D and full 2D.
Apart from increasing the number of cluster sites, a natural extension is to consider hoppings not only in one dimension but also perpendicular to it. By copying the 1D-Hubbard chain and coupling the clusters perturbatively to its new neighbors, a semi-2D lattice tiling is achieved (see Fig. 3.1).

The next step is to consider 2D-shaped clusters, the smallest of which being quadratic and containing four lattice sites. This is further extended to a rectangular 2x3 or 3x2 cluster of six sites. Any further increase in the size of the single cluster treads on the limits of full diagonalization techniques as well as the maximal size of matrices that have to be kept in memory during the CPT calculation and would require the implementation of approximative cluster solvers, such as Lanczos methods, which is beyond the scope of the present work.

Most of our calculations were carried out at half-filling (hf.) with time steps of $d\tau = 0.03$ if not stated otherwise.

5.2.1 Convergence

For the 1D Hubbard model convergence is reached rather rapidly with respect to the number of clusters as depicted in Fig. 5.1 where the interaction was set to $U = 2$ and the external field strength is $E = 2$. The results for $N_c = 10$ and $N_c = 30$ differ only slightly and a further increase to $N_c > 30$ does not produce any visible changes in the data.

However, a more significant difference is discernible on behalf of the cluster size. The 2-site cluster is a very strong and rather crude approximation because in 1D only one half of the total couplings between neighboring sites is considered exactly, the other half is treated perturbatively. It can be expected that considering 4 sites per cluster is already a sharp improvement in terms of accuracy.

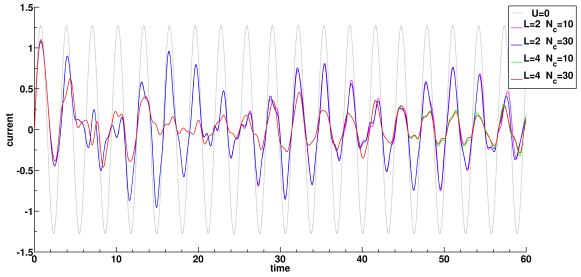

Figure 5.1: Convergence pattern for the 1D atomic chain. Calculations were carried out at hf. with $E = 2$, $U = 2$, number of clusters N_c on the lattice and different cluster sizes as indicated. The black line for the noninteracting case was calculated analytically and serves as a reference frame.

The 2D results for the same configuration ($U = 2$, $E_0 = 2$) are shown in Fig. 5.2.
For the quadratic 2x2 cluster the results are not fully converged in the case of a lattice consisting of 20x20 clusters (i.e. 1600 sites) but convergence is good enough (as can be inferred from the relatively minor changes between N_c =17x17 and N_c =20x20) to produce reliable results.
Simulations become very time expensive as the number of clusters increases, e.g. when the lattice is expanded from 1600 (N_c =20x20) to 2304 (N_c =24x24) sites, while little is gained in accuracy of the data. Especially, since possible improvements are only achieved quantitatively and leave the results qualitatively unchanged.

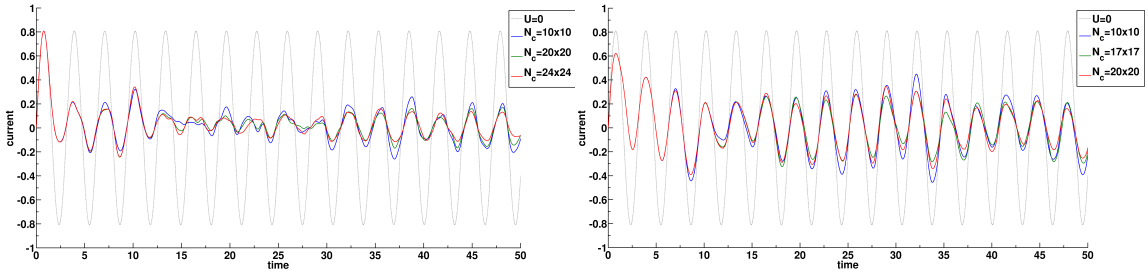

(a) (b)

Figure 5.2: Convergence performance in 2D at $E_0 = 2$, $U = 2$, (a) for a linear 4-site cluster , (b) for a quadratic 2x2 cluster.

In the case of 6-site clusters, the CPT procedure is limited to comparatively small superlattices of about N_c =12x12, in order to keep the computational time to complete the calculations within reasonable means. Although this means a loss in accuracy with respect to the evaluation of the Brillouin zone, there is also a significant gain in terms of accuracy by increasing the number of hoppings that are treated exactly.
One additional limitation with regard to computer memory stems from an exponentially growing Hamilton matrix for the single cluster that has to be diagonalized, another is posed by the amount

of time that is needed to calculate the time evolution and the contribution of each wave vector to the current.

Another problem arises when considering large time scales: Since the time step for the midpoint time evolution scheme as delineated in Sec. 3.4.2 has to be kept sufficiently small to ensure that the systematic error has little impact on the outcome, the only way to reach large times is to increase the absolute number of time steps. But as the numerical error piles up the time evolution operator is loosing its unitarity after many iterative steps and individual outliers in the matrix elements may lead to additional oscillatory behavior and thus distort the results.

5.2.2 1D and 2D specifics

First we consider a one-dimensional chain of atoms with a total of about 80 to 120 lattice sites, depending on the size of the individual clusters. For CPT the lattice is tiled into clusters with either two, four or six sites per cluster resulting in superlattices that consist of 40 clusters in the first case and 20 clusters in the other two.

When we move up to two-dimensional lattices, the total amount of cluster sites on the superlattice increases sharply due to the second dimension. A reasonable trade-off between accuracy, i.e. resolution in momentum space, and computation time can be inferred from convergence calculations. For most of the results given in this chapter a size of 17x17 clusters is used for the superlattice of two- and four-site clusters and 12x12 for six-site clusters, which amounts to a total lattice of roughly 600 or 1200 sites in the case of the smaller clusters and nearly 900 in the latter case.
Although the lattice sizes are comparatively similar, the results in terms of accuracy improve significantly with larger cluster sizes. For a comparison of the effects of different lattice tilings on the current density see Figs. 5.3 and 5.4.

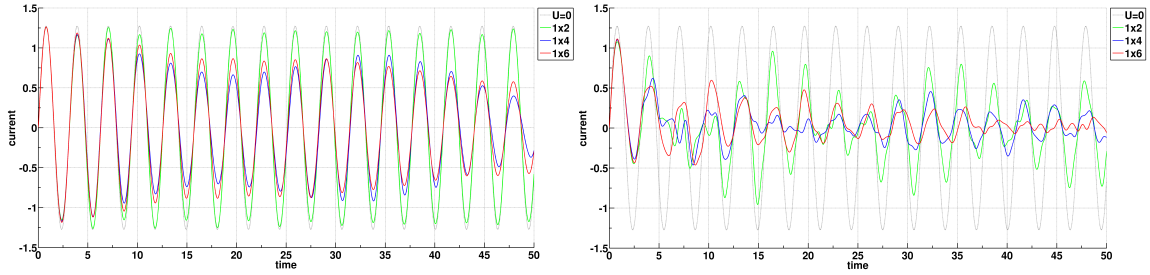

(a) (b)

Figure 5.3: Comparison of the current density in a 1D chain for different cluster sizes of 2, 4 and 6 sites respectively, $E_0 = 2$, the interaction strength is set to (a) $U = 0.5$ and (b) $U = 2$.

Besides the prominent Bloch oscillations with a period of $T_B = \frac{2\pi}{E_0}$ the current density exhibits a damping of the current as soon as the interaction is turned on. This quenching of the oscillatory behavior is enforced when the cluster grows larger, as can be seen in 1D (Fig. 5.3) as well as in 2D (Fig. 5.4) for interaction strengths $U = 0.5$ and $U = 2$.

Also noticeable, in the $U = 2$ case smaller clusters tend to maintain the periodicity of Bloch oscillations throughout the whole time frame, whereas the 2x3 cluster shows irregular behavior

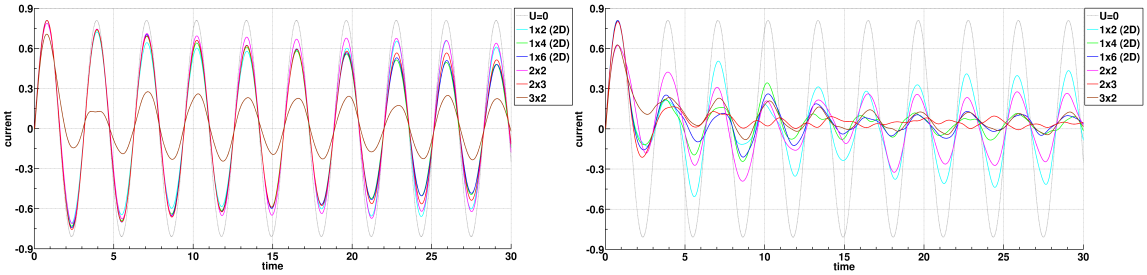

(a) (b)

Figure 5.4: Comparison of the current density on a 2D lattice for different cluster sizes and shapes, $E_0 = 2$, the interaction strength is (a) $U = 0.5$ and (b) $U = 2$.

already after about three cycles. During this initial oscillations the damping effect is most severe but abates for larger times. Due to the limited time range of the simulation, it is not clear whether the current density eventually goes to zero or to some non-zero constant value and the system approaches a steady state. However, there are indications that some (irregular) oscillatory patterns remain also for very large times.

Fig. 5.5 displays on the one hand the time dependence of the current density for different electric field strengths (increasing E_0 from 0.25 in panel (a) to 2 in panel (d)) and on the other hand the effects of small or large on-site interactions. The Bloch frequency is directly proportional to the external field leading to rapid oscillations for large E_0.

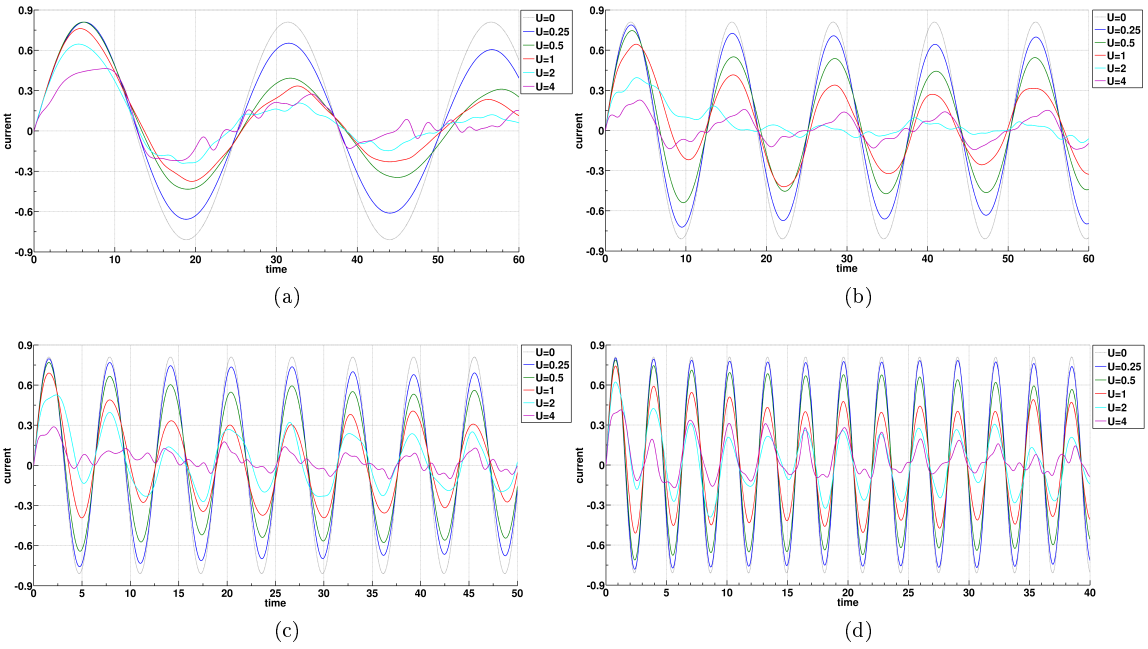

(a) (b)

(c) (d)

Figure 5.5: Current density at different interaction strengths for quadratic 2x2 clusters with a field amplitude of (a) $E_0 = 0.25$, (b) $E_0 = 0.5$, (c) $E_0 = 1$ and (d) $E_0 = 2$. Note the different time scales.

The Bloch oscillations in the case of metallic systems, that is for rather small electron-electron correlations ($U < 1$), are exactly matching the periodicity of the ideal, noninteracting case with the exception that the amplitude is declining over time.
At around $U = 1$ the oscillations are deformed and additional oscillations appear on top of the original ones. These extra patterns start out as small wiggles and become progressively dominant as the correlation strength increases. This process occurs slowly and is not a distinct point-like transition.

The oscillations become to a greater extent irregular as U increases. Large correlations also mean that the system is eventually turning into a Mott insulator.
The current gets more and more suppressed as correlations between particles increase. For metallic systems the decay of the amplitude can be interpreted as an augmentation in scattering events that hinder the movement of electrons through the lattice.
For example, in panel (c) of Fig. 5.5 the current for the $U = 4$ case is sharply damped after the first half of the Bloch period, whereas for small electron-electron interactions the quenching of the Bloch oscillations is less intense.

A larger electric field provokes a stronger response by the system and drives the current for a longer period of time as can be seen in Fig. 5.5 when comparing the strong damping of the blue line ($U = 0.25$) for $E_0 = 0.25$ as opposed to a slight damping for $E_0 = 2$.

Note that even for large external fields, linear response theory is valid as long as, in the case of a static field, $E_0\tau$ is very small compared to the Bloch period.

5.3 DMFT results for the Falicov-Kimball model

The following section is intended to provide at least a qualitative comparison to results that were recently obtained from Dynamical Mean-Field Theory (DMFT) calculations by J. K. Freericks and others.
We will not give a detailed account of their findings nor of the particulars of DMFT. An elaborate discussion of the numerical results can be found in their papers, Refs. [9, 25, 45, 61, 62], and a comprehensive description of the spinless Falicov-Kimball model is given in Ref. [27].
In all numerical calculations the authors consider the case of half-filling with particle densities of both the itinerant and localized electrons equal to 1/2 and the same chemical potential for both sorts of electrons.

Although the Hubbard and the FK models have distinct features of their own, they both are capable of describing general physical phenomena in strongly correlated materials, such as Bloch oscillations and the damping of the current, in a comparable way.

The adopted results for the FK model's nonequilibrium current response to an external electric field are given in Fig. 5.6. The same damping effects occur, as we have seen in the previous section, for increasing coupling strengths. The damping becomes so severe that the current density does not complete a full Bloch period if U lies within the Mott insulating regime $U > U_c$.
Additionally, beat-like phenomena arise in the case of metallic systems (see especially the upper panel of (b) in Fig. 5.6). This is to some extent also seen in the Hubbard model, though the pattern is much less regular and seems to depend rather strongly on the cluster size (cf. Figs. 5.3, 5.4).

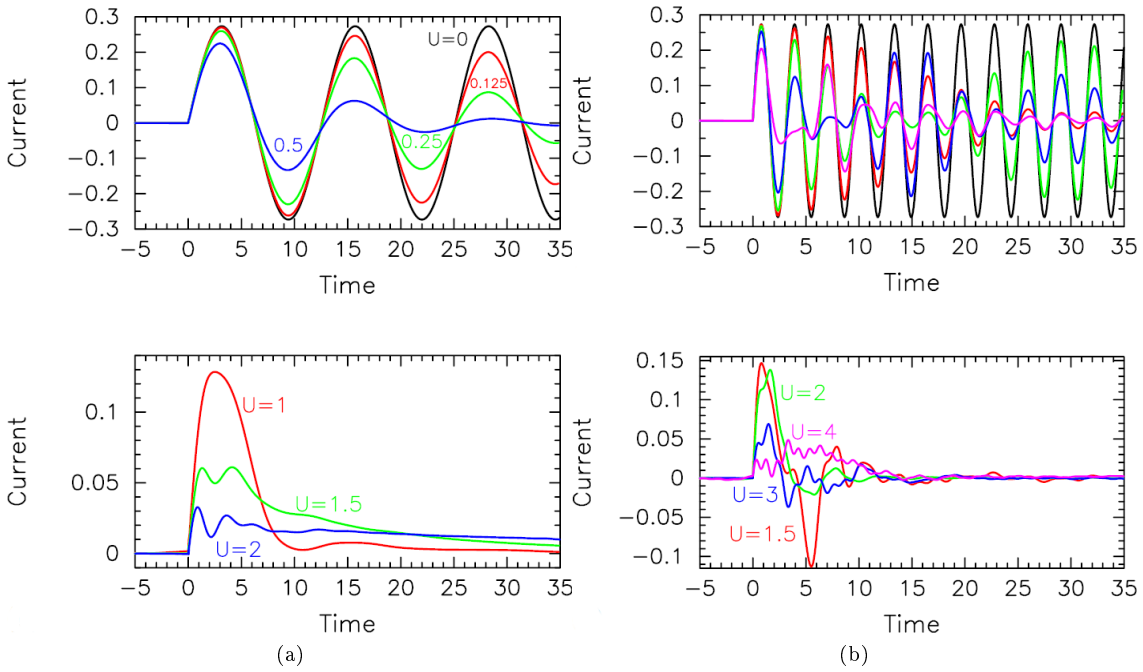

Figure 5.6: DMFT results for the FK model, adopted from [25]. Metallic systems are displayed in the upper panels, Mott insulators in the lower panels. The equilibrium FK model in infinite dimensions features a MIT at $U_c = \sqrt{2}$. Results are plotted for (a) $E_0 = 0.5$, (b) $E_0 = 2$ and U as indicated.

According to [25] these beats, which seem to have a periodicity of $2\pi/U$, become increasingly visible for large electric fields and can be attributed to two sharp peaks in the density of states centered at $\pm U/2$.

A beat period inversely proportional to the interaction strength was predicted for the tight-binding Hubbard model in [63]. The authors carried out nonequilibrium calculations of the correlated motion of two electrons in a one-dimensional lattice, showing the occurrence of oscillations in the drift velocity of the particles.
For a uniform external electric field the periodicity turned out to be h/U (which translates to $2\pi/U$ in atomic units) depending only on the interaction strength U and being independent of the hopping amplitude t.

For small field strengths the current density in the case of Mott insulators (see lower panel of Fig. 5.6a) seems to approach a non-zero steady state solution. However, as the authors mention in [9], a steady state response in a perturbative approach is difficult to determine accurately and further complicated by the limited time window of the calculations.

5.4 Results from t-DMRG calculations

The density matrix renormalization procedure was first proposed by S. White in 1992 [29] and has gained importance alongside increasing computer power ever since. For a comprehensive review of the DMRG method see for example Ref. [64].

Very recently the adaptive time dependent density matrix renormalization group (t-DMRG) approach was introduced as an extension to DMRG and a powerful numerical approach to one-dimensional, strongly correlated systems driven out of equilibrium (see Ref. [65]).
Note, in contrast to CPT and DMFT, DMRG methods are basically exact although limited by computational resources and confined to 1D models.

Most t-DMRG calculations use a one-dimensional chain with pbc, i.e. a ring of atomic sites, to which a magnetic field is applied in order to model an electric current flowing through the system. A different way to introduce an electric field than by incorporating Peierls' substitution for the hopping amplitude is therefore by means of Faraday's law, resulting in a circular electromotive force. A time dependent Aharonov-Bohm flux $\Phi'(\tau) = e\Lambda a E\tau$ is piercing the ring-shaped 1D lattice and the Hamiltonian for the corresponding Hubbard model takes on the form [66]

$$\hat{H} \;=\; -t\sum_{i,\sigma}\left(e^{\mathrm{i}\,\Phi(\tau)}c^{\dagger}_{i,\sigma}c_{i+1,\sigma} \;+\; \text{h.c.}\right) + \; U\sum_{i} n_{i\uparrow}n_{i\downarrow} \tag{5.6}$$

where $\Phi(\tau) = \Phi'(\tau)/2\pi\Lambda = E\tau$ (in units of $e = a = 1$) is a time dependent phase equivalent to the Peierls phase that was introduced in Sec. 3.3.

The most interesting result from t-DMRG calculations is a breakdown of the Mott insulating phase for strong electric fields which is dependent on the magnitude of the electron-electron interaction. If E_0 becomes large enough the system shows an increase in the current response and again turns into a metal, thereby destroying the Mott insulating state.
The breakdown is indicated by a gradually developing decay rate of the ground state [46] as tunneling to excited states is enhanced when the eletric field strength increases.

The dielectric breakdown of a band insulator is well understood in terms of Landau-Zener tunneling that arises between the valence and the conduction band. The main difference now to a Mott insulator is that the excitations across the band gap can move freely in a band insulator whereas in the presence of a Mott gap they are bound to interact with other electrons.

T. Oka and H. Aoki [46, 66] managed to show that the dielectric breakdown of the 1D Mott insulator can be explained according to the same considerations as in the case of a band insulator. An extension of the Landau-Zener mechanism works fine also for correlated many-body systems if the band gap is replaced by the charge gap of the Mott insulator.
It should be noted that the authors of another t-DMRG study [48] in which they are using a different setup did not find the same strong indications that the breakdown of the Mott insulator could be attributed to the Landau-Zener mechanism. Instead of modeling the electric field with the help of a magnetic flux through a ring, as mentioned above, the authors were looking at a 1D Hubbard chain to which a static bias voltage is applied.

Nevertheless, both studies found the breakdown occurring as soon as the field strength exceeds the energy gap and a current similar to the one in the breakdown regime of a band insulator arises.

Others [47] have looked at a single cluster of four sites and applied an electric potential to two noninteracting leads that are attached to the interacting region in between. The bias voltage drives the system out of equilibrium and above a certain threshold voltage the Mott insulator breaks down. In this case, for large times a steady state current can be observed.

Due to the limitations posed by the accessible time window in our CPT calculations, we are not able to reach a steady state. Therefore, it is not possible for us to determine the dependence of steady state currents on the strength of the electric field in the face of a Mott insulator breakdown. Nonetheless, we may get a hint from averaging over the oscillation pattern at long times as to whether the current tends towards zero or rather a finite value. The latter would be an indicator of the dielectric breakdown.
It is necessary to consider only data well beyond the transient phenomena at small and medium times to get into a regime that is close to the steady state.

The long-range performance of the 1D current density is portrayed in Fig. 5.7. As long as the magnitude of the electric field is larger than the Mott gap, which is roughly the case when $U < E_0$ for small interactions up to $U = 1$, the Bloch oscillations exhibit a fairly regular behavior. This is the metallic regime and the damping reaches out over many Bloch cycles.
In the region near the insulator breakdown, where E_0 is slightly smaller or larger than the gap size (see both cases of $U = 0.75$ in panels (a) and (b) for example), the oscillations are losing their characteristic periodicity. Although a periodic order is still discernible, the oscillations are clearly shifting away from the $U = 0$ reference.
When the correlation strength is further increased, the system turns into a Mott insulator and the current response is damped rather strongly, for instance in the case of $U = 3$ in panel (b).
In panel (c) the Mott gap becomes larger than the external field at about $U \geq 6$.

Summing up, the current density oscillates regularly in the areas where the electric field dominates the electron-electron correlations and a continuous damping of the amplitude occurs. For strong interactions, i.e. if the Mott gap exceeds the magnitude of the electric field, the Bloch oscillations evolve into an irregular pattern and are damped more sharply, especially within the first few Bloch periods.

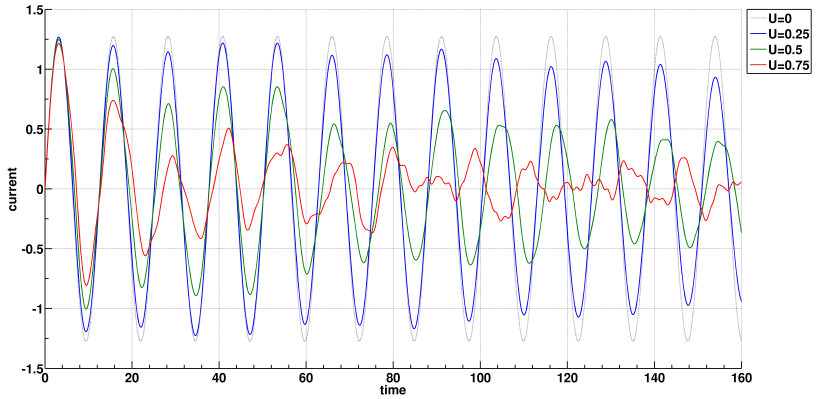

(a)

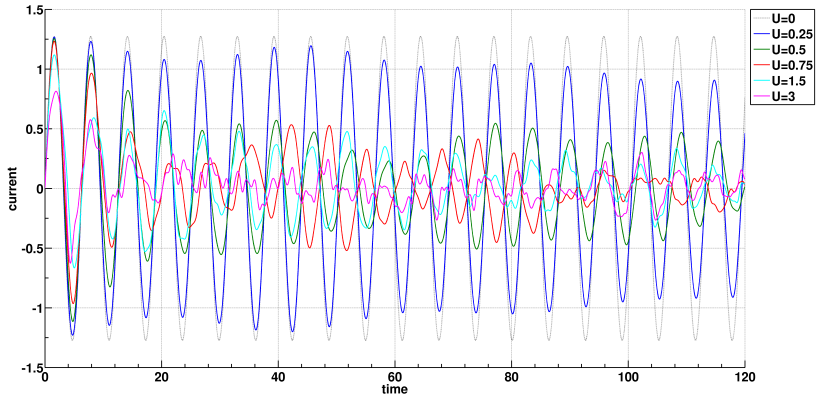

(b)

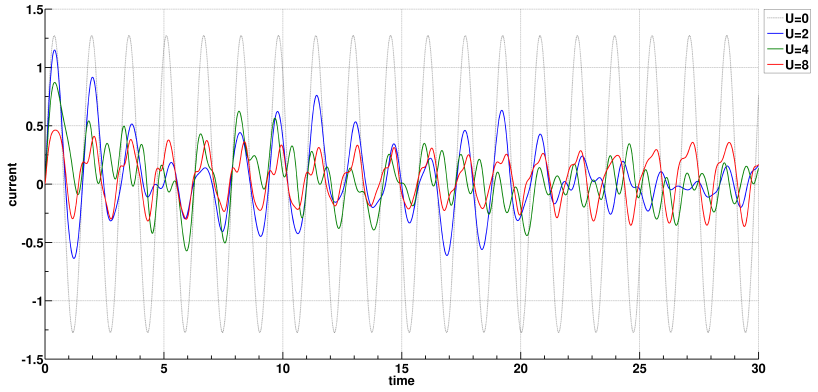

(c)

Figure 5.7: 1D current density (6-site clusters) in the long-range regime for different on-site interactions. The magnitude of the electric field is (a) $E_0 = 0.5$, (b) $E_0 = 1$, (c) $E_0 = 4$.

5.5 Oscillating electric fields

We now turn our attention to periodic external fields that may be written generally as a sum of a static and an alternating field, such that

$$E(\tau) = E_0 + E_1 \cos(\omega\tau) \tag{5.7}$$

The frequencies considered here lie in the same range as the characteristic frequency of Bloch oscillations, i.e. they are of the order of about 10^{13}Hz. It is still a technical challenge to produce powerful sources of terahertz radiation. Recent developments show the possibility of using alternating currents in Josephson junctions to provide electromagnetic fields whose frequency can be adjusted by the applied voltage to the terahertz regime [67].
Another way of realizing such frequencies could be the usage of a second device whose Bloch oscillations, generated by a static field, would in turn create an alternating field and thus drive an oscillating current in the first system.

With a purely oscillating electric field present, i.e. $E_0 = 0$, the Bloch oscillations are driven by the frequency ω of the E-field and not by the magnitude of the field as in the static case, thus resulting in a periodicity $T_{B'} = 2\pi/\omega$.

Altering the frequency of the driving field produces a large variety of oscillation patterns, examples of which are given in Figs. 5.8 and 5.9.

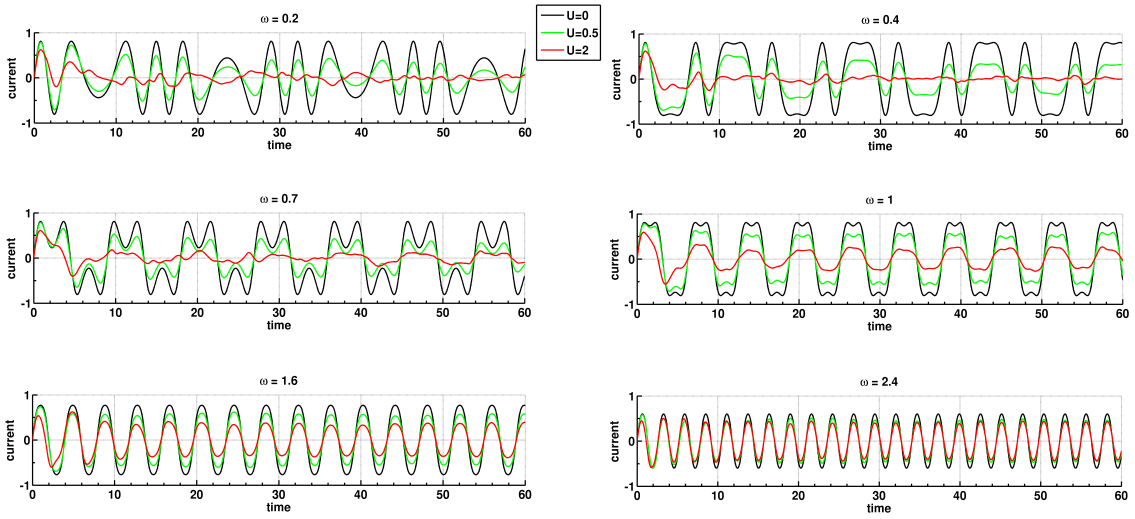

Figure 5.8: Oscillation pattern for different driving frequencies of an external field $E = 2\cos(\omega\tau)$ with $U = 0.5$ and $U = 2$.

If the magnitude E_1 of the oscillating field is changed, the periodicity of the Bloch oscillation remains fixed at $T_{B'} = 2\pi/\omega$. A difference occurs only in the modulation pattern of the oscillations. With increasing E-field magnitude the current density within a single Bloch period does oscillate more frequently as compared to small values of E_1.
For example, in the case of $E = 2\cos(0.4\tau)$ (see upper right panel in Fig. 5.8) the Bloch period equals $T_{B'} = 5\pi$ and encompasses four peaks in the current density. The results for a field with smaller magnitude $E = 1\cos(0.4\tau)$, in contrast, show only two peaks in the same region.

In summary, the periodicity of the system's response to the driving field is determined by the frequency ω of the external field, whereas the frequency of the over-all oscillatory behavior within the Bloch period is proportional to the field strength E_1.

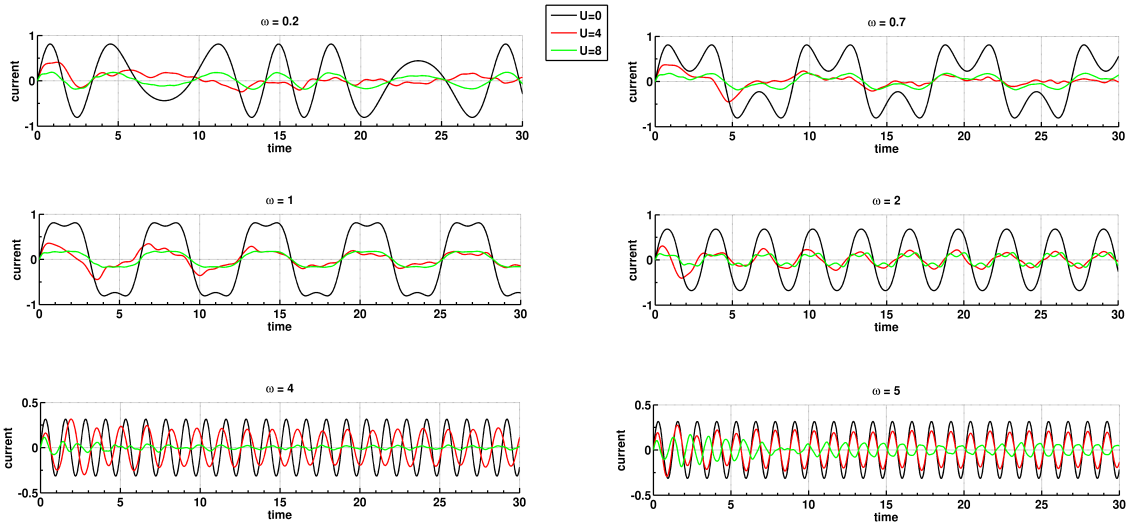

Figure 5.9: Oscillation patterns for different driving frequencies of an external field $E = 2\cos(\omega\tau)$ with $U = 4$ and $U = 8$.

The maximum amplitude that is reached by the current is reduced for large driving frequencies as can be seen in the lower right panel of Fig. 5.8. At large frequencies the electric field has not enough time to fully establish. Interestingly, as the frequency is further increased the CPT results seem to match the current response of a noninteracting system.
In fact, this occurs only for small or medium interaction strengths. When we probe very strongly interacting systems, the suppression of the current is substantial enough, so that the maximal current in the interacting case is still well below the (reduced) amplitude of the noninteracting case.
See also Fig. 5.10 for the case of $E = 1\cos(3\tau)$ and two interaction strengths $U = 2$ and $U = 8$. Notice the reduced maximal amplitude from about $j_{\max} = 0.8$ when ω is rather small to $j_{\max} = 0.26$ in the case of $\omega = 3$.

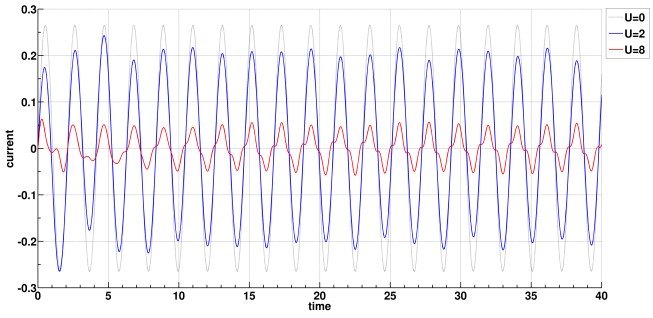

Figure 5.10: Reduction of the noninteracting amplitude (black line) and suppression of the current for $U = 2$ and $U = 8$ under the influence of $E = 1\cos(3\tau)$.

The decay of the noninteracting amplitude occurs at a critical value ω_c of the driving frequency. It also depends linearly on the magnitude of the electric field. Fig. 5.11 depicts the amplitude reduction as a function of the applied frequency for different field strengths.
The onset of the amplitude reduction is indicated for larger fields and follows the relation $\omega_c = \frac{2}{\pi}E_1$.

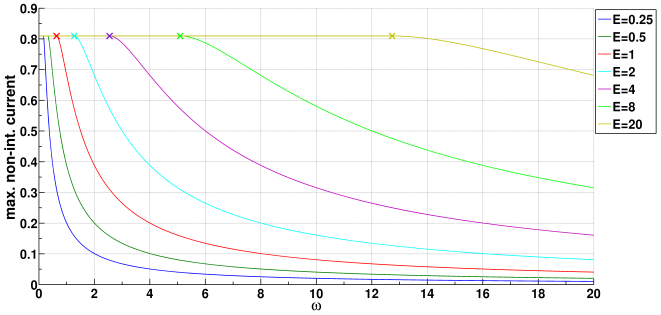

Figure 5.11: Decay of the maximal amplitude for the noninteracting current as a function of ω. Also shown is the dependence of ω_c (indicated with a star) on the magnitude E of the applied electric field $E(\tau) = E\cos(\omega\tau)$.

5.5.1 Enhancement phenomena

What happens if a multiple of the driving frequency ω coincides with the Bloch frequency ω_B?
For medium interaction strengths and magnitudes of the electric field there seems to occur an increase in the current if the driving frequency is close to the Bloch frequency, see $U = 4$ case in panel (a) of Fig. 5.12. If the frequency is small, then the damping is dominant and for large frequencies or cases where the amplitude of the E-field is much bigger than U, no such enhancement is observable (panel (b)).
It cannot be ruled out that the rather small size of the clusters has a possibly significant influence on the partial development of enhancement patterns in the current density.

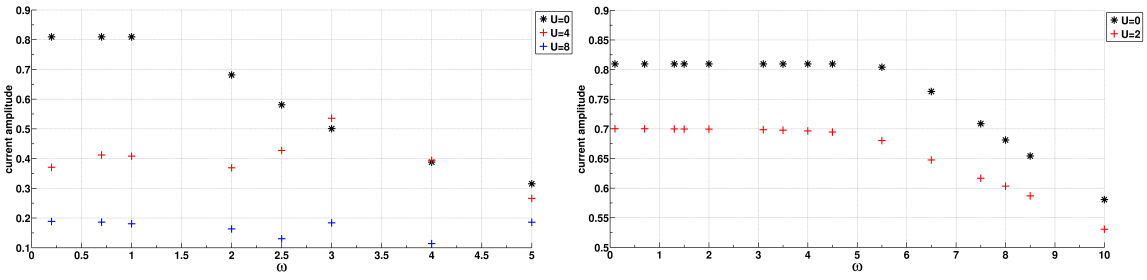

(a) (b)

Figure 5.12: Decay and partial enhancement of the maximal amplitude for the interacting current as a function of the driving frequency ω. The electric field is given by (a) $E(\tau) = 2\cos(\omega\tau)$ with $U = \{4, 8\}$ and (b) $E(\tau) = 8\cos(\omega\tau)$, $U = 2$.

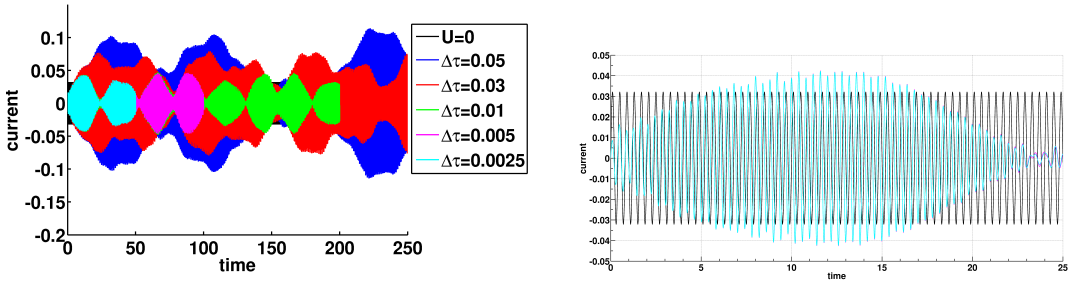

(a) (b)

Figure 5.13: Influence of the size of the time steps $\Delta\tau$ and development of unphysical amplification of the current for a 2-site cluster in 1D, $E = 0.4\cos(5\pi\tau), U = 4\pi$. (a) For smaller $\Delta\tau$ the data seems to converge towards beats which have a period of 8π. (b) Although the data has converged, the current density grows beyond the noninteracting maximum.

In a different situation, the finite cluster approximation and the discretization in time that introduce some amount of inaccuracy may cause an incorrect amplifaction of the current for a certain combination of parameters. Fig. 5.13 gives an example of how significant a role the cluster size and the resolution in time can play in CPT calculations. The current density is highly oscillating due to a very large driving frequency of $\omega = 5\pi$. Panel (a) gives a qualitative picture of the overall behavior of the current, where the colored areas are actually high frequency oscillations as can be seen in the larger resolution of panel (b).
In the case of the largest time steps a sharp increase beyond the noninteracting case (in black) can be observed which is of course unphysical. The results get slightly better with smaller time steps, but even if $\Delta\tau$ is reduced to less than one-tenth of its original value, the current response exceeds the $U = 0$ maximum.

This phenomenon seems to arise most prominently in the 1D chain for small clusters and only for certain parameters, that is, if the driving frequency ω is a multiple of π and U is of the same order as ω.

The boost in the interacting current is persistent in 1D regardless of the size of the cluster and occurs at certain pathological combinations of U and ω also for the smallest two-dimensional cluster but vanishes completely when we consider a 2x3 or 3x2 configuration, see Fig. 5.14.

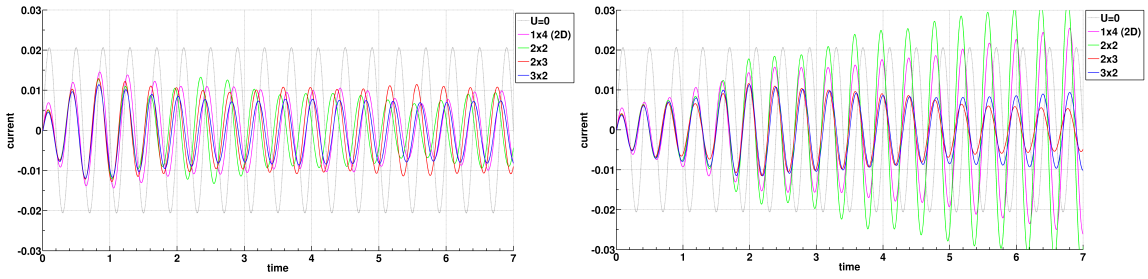

(a) (b)

Figure 5.14: Current density for different clusters at $E = 0.4\cos(5\pi\tau)$ and (a) $U = 5\pi$, (b) $U = 6\pi$.

For certain combinations of E_1, ω and U transient phenomena appear at the beginning when the external field is turned on. The frequency of the Bloch oscillations shifts a little bit to higher values. After a few cycles have been completed the current density again oscillates in phase with the non-interacting result.
This can be seen for example in Fig. 5.9 in the two panels at the bottom and also in Fig. 5.14. The larger the electron-electron correlation the bigger is the shift away from the Bloch frequency in the beginning.
This may be explained with regard to a harmonic oscillator which would be expected to react with a phase shift to a resonant external field.

5.5.2 Static plus oscillating field

We are now considering a superposition of a static and an oscillating electric field according to equation (5.7) with finite magnitudes E_0 and E_1.
The overall behavior of the current density is very much alike the phenomena discussed in the previous sections. For comparison a couple of examples are presented in Fig. 5.15.

On the one hand the amplitude of the static field exactly determines the periodicity of the Bloch oscillations, $T_B = 2\pi/E_0$, when the driving frequency ω takes on an integer value. On the other hand if ω is some rational (or irrational) number the oscillatory behavior of the current response is still dominated by T_B, but the shape of the individual Bloch cycles becomes irregular though not entirely random. The irregular patterns too show large periods after which the pattern is repeated again. For example, this can be seen in on the left hand side of Fig. 5.15 for driving frequencies $\omega = 1.6$ and $\omega = 2.8$ where the irregularly shaped Bloch oscillations are reproduced after a period of 10π.

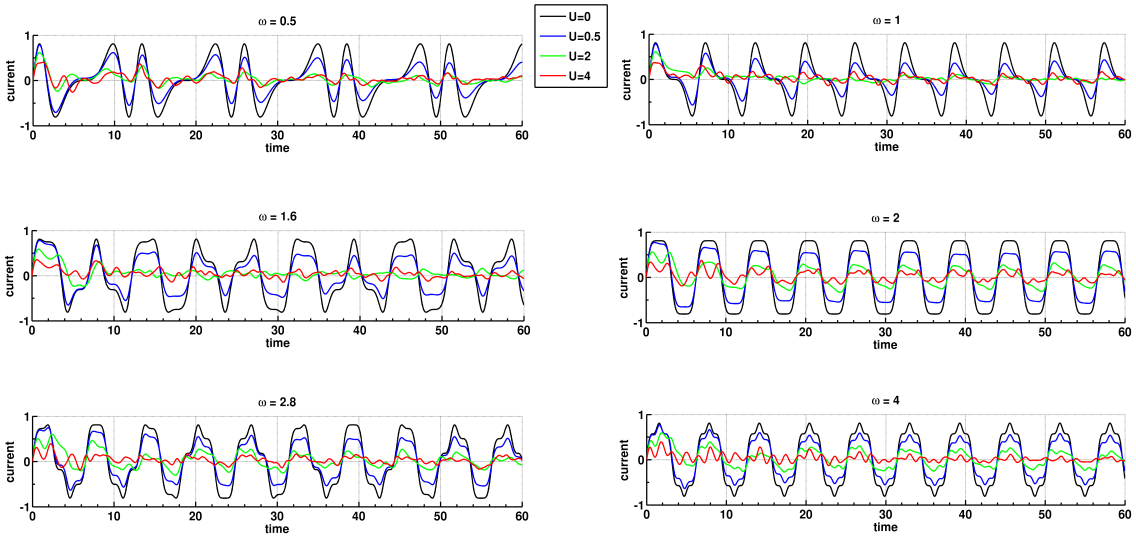

Figure 5.15: Oscillation patterns for different driving frequencies ω of an external field given by $E = 1 + 1\cos(\omega\tau)$. The interaction strength is ranging from the metallic regime for $U = 0.5$ to a Mott insulating regime for $U = 4$. Note that on the right hand side the Bloch oscillations are perfectly regular and period is $T_B = 2\pi$ for all configurations due to the driving frequency being equal to an integer value.

E_1, the magnitude of the alternating field, predominantly affects the system's response within each Bloch period. While the periodicity stays the same, large recurrent fields lead to additional oscillations superimposed on the underlying Bloch oscillations. As a result the Bloch oscillations may consist not only of one peak, which is the case for small E_1, of several distinct peaks when $E_1 > 1$. For instance, the current driven by an electric field $E = 1 + 4\cos(\omega\tau)$ is depicted in Fig. 5.16 for some selected values of ω. A comparison of this to the results in Fig. 5.15 clearly shows the additional oscillations arising from the change in E_1.

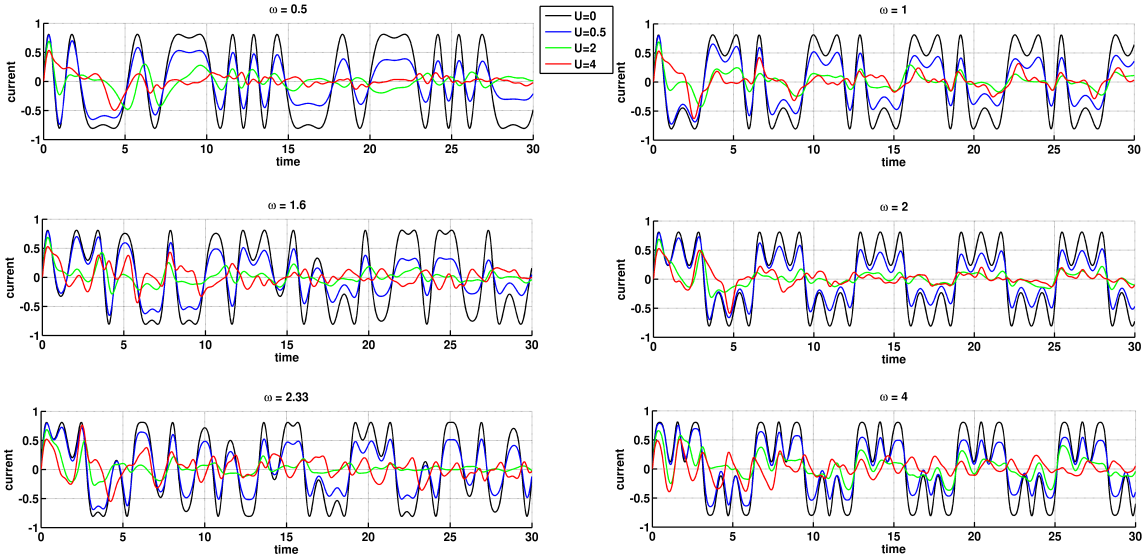

Figure 5.16: Oscillation patterns for different driving frequencies ω of an external field given by $E = 1 + 4\cos(\omega\tau)$ and interaction strengths $U = 0.5, 2$ and 4.

5.6 Band doping

By shifting the chemical potential away from its value of $\mu = U/2$ at exactly half-filling, one can achieve a certain degree of electron or hole doping. For relatively small changes of μ the clusters themselves remain undoped because the chemical potential still lies within the energy gap.
Changing the chemical potential to values far away from half-filling and outside the gap would eventually lead to cluster doping where an additional electron or hole is present in each cluster.

The gap between two energy bands of the whole lattice that are formed by coupling the individual clusters is smaller than the Mott gap of a single cluster. Thus, band doping occurs while the clusters, with regard to actual particles, remain undoped.
We are only considering the case of hole-doping ($\mu < U/2$) here. However, the results are entirely equivalent to the situation of particle-doping where the chemical potential is taken above its value at half-filling ($\mu > U/2$) because of the particle-hole symmetry of the Hamiltonian.

The effects of band doping are only significant if the external electric field is much smaller than the interaction strength. $E \ll U$ means that the system is well within the Mott insulating regime. Since the energy gap in a Mott insulator is a charge gap, introducing additional charge carriers causes the system to become more metal-like. As expected, the consequence is an augmentation of the current.

In Fig. 5.17 the cases for static electric fields of magnitude $E_0 = 0.2$ and $E_0 = 1$ as well as on-site interactions $U = 4$ and $U = 2$ are depicted for various chemical potentials ranging from no doping at half-filling to large doping near the band edge.

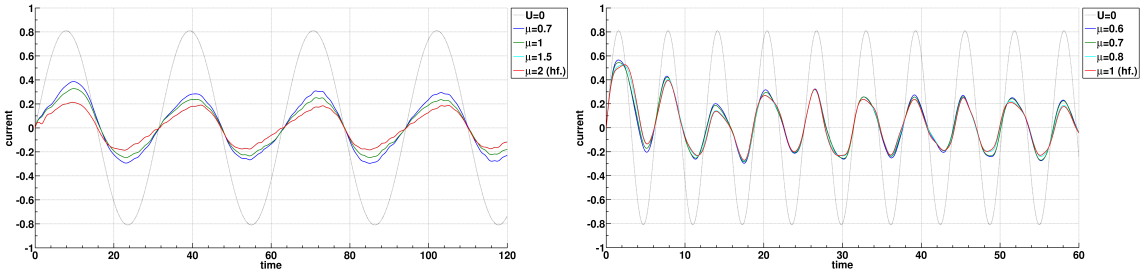

(a) (b)

Figure 5.17: Band doping for a system in a static external field. Parameters are (a) $E = 0.2$, $U = 4$, and (b) $E = 1$, $U = 2$. The results for the smallest chemical potential ($\mu = 0.7$ and $\mu = 0.6$ respectively) lie very close to the band edge where cluster doping would occur.

As the doping increases the system becomes more and more metallic in character. This is clearly visible in the increased amplitude of the Bloch oscillations.

For large electric fields (that is, if E is of the same order as U) doping does not have a significant effect with respect to the current. The very short periodicity of the Bloch oscillations prevents a strong damping caused by U.

Doped bands in a driving field

The extension to an alternating external field is straightforward. With regard to the effects of band doping, the results do not depend specifically on the nature of the electric field. As seen before, a small shift of the chemical potential away from its value at half-filling does not change the properties of the system. If the chemical potential is further decreased below (or increased above) $\mu = U/2$ the system turns away from its Mott insulating properties and behaves more like a metal.

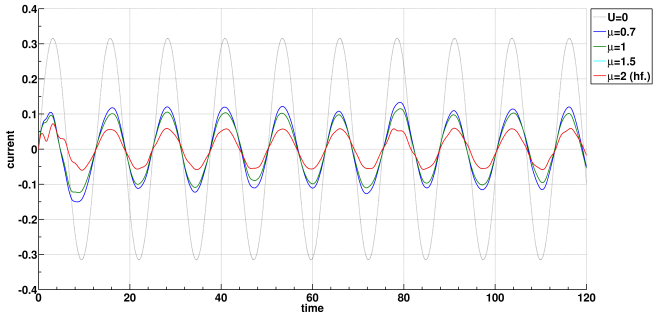

Figure 5.18: Band doping for 2x3 clusters in an oscillating external field $E = 0.2\cos(0.5\tau)$, $U = 4$. Note, the scale for the current axis has changed compared to Fig. 5.17.

In Fig. 5.18 the time resolved current density of a two-dimensional lattice with electron-electron correlation energy $U = 4$ is shown as a periodic field $E = 0.2\cos(0.5\tau)$ is applied.

A superposition of static and periodic fields produces a different and generally more complex shape of the noninteracting Bloch oscillations. Since in Fig. 5.19 the interaction strength is one order of magnitude larger than the amplitude of the electric field, the damping effects of the Bloch oscillations dominate.
This in turn yields an interacting current that does not resemble the same specific shape. However, when the system acts more like a metal the damping becomes less severe and the current again takes on some of the features of its noninteracting counterpart. Most prominently this can be seen in panel (a) by comparing the case of half-filling (red line) and the case of heavy doping (blue) with the noninteracting result (black).
Notice the large Bloch period of 10π in all three images of Fig. 5.19.

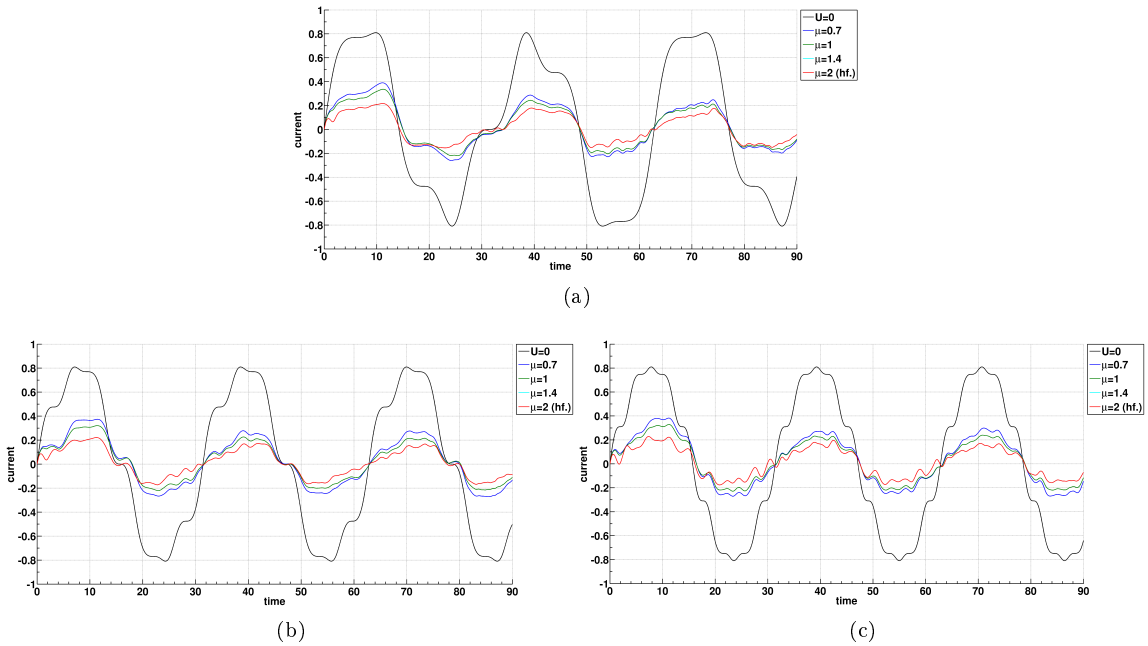

(a)

(b)

(c)

Figure 5.19: Band doping for 2x3 clusters in a superposition of a static and an oscillating external field $E = 0.2 + 0.2\cos(\omega\tau)$ with varying driving frequency, (a) $\omega = 0.5$, (b) $\omega = 1$, (c) $\omega = 1.6$. The interaction is set to $U = 4$ in all cases. Note, the data for $\mu = 1.4$ (cyan) overlaps almost exactly with the results at half-filling (red).

Chapter 6

Conclusions

In strongly correlated materials the competition of kinetic and potential energy, which are both of about the same order of magnitude, lead to various interesting properties. Standard models in condensed matter physics are not capable of describing these phenomena properly and new approaches have to be established.
Starting from the fermionic Hubbard model we developed a pseudoparticle description within the framework of Cluster Perturbation Theory (CPT).

The system starts in equilibrium and then a strong external electric field is turned on that drives a current. We focused on the time evolution of the current density and investigated the influence of electron-electron correlations on the damping of the Bloch oscillations in one-dimensional and two-dimensional systems. Increasing the Coulomb repulsion among transient particles reduces the amplitude of the oscillations more rapidly as the system exhibits Mott insulating behavior.
We found qualitative agreement of our results with calculations obtained by Dynamical Mean Field Theory (DMFT) for the Falicov-Kimball model and by time dependent Density Matrix Renormalization Group (t-DMRG) for an atomic ring.

The extension to periodic fields reveals additional effects on behalf of the Bloch frequency. Bloch oscillations occur with a characteristic frequency proportional to the magnitude of a static electric field or, in the case of an alternating E-field, the oscillations are driven by the field's frequency.
Strong interactions lead to a quick diminishing of the Bloch oscillations and an irregular highly oscillatory evolution of the current density.

We pointed out the differences between conventional band insulators and Mott insulators and discussed the formation of the Mott gap as well as the potential dielectric breakdown of the Mott insulating phase at large field strengths.

We also examined the case of band doping which, if sufficiently far away from half-filling, increases the metallic behavior of the system by changing the carrier concentration.

From the comparison with DMFT and t-DMRG it is apparent that CPT is a promising and valuable alternative to very time- and memory-expensive techniques, yielding valid results at much less cost. An additional advantage with regard to DMRG is that the extension to more than one dimension is straightforward in an approach based on CPT.

As CPT is one of the simpler quantum cluster methods, it can be refined for example by adding additional fields or bath degrees of freedom to the cluster. This leads eventually to methods like Variational Cluster Approximation (VCA), Cluster Dynamical Mean-Field Theory (C-DMFT) or the Self-Energy Functional Approach (SFA), where variational or self-consistency principles are

applied to evaluate the additional parameters. For more details on these approaches see for instance [34] and references therein.
One avail of these cluster methods is the possibility of studying long-range ordering phenomena and broken symmetry phases which, due to its one-step nature, cannot be analyzed by means of CPT.

At present the direct observation in an experimental setup of the phenomena described here is not achievable. On the one hand most solid state systems where Bloch oscillations are detectable are multi-band structures. The presence of a large field will induce Zener tunneling to higher energy bands which we neglected. On the other hand, ultracold atoms trapped in tunable optical lattices, which are the experimental equivalent to the Hamilton gauge in our model, can serve as an authentic realization of the kind of systems we investigated. Unfortunately, strict temperature requirements and the necessity of reconstructing the current from time-of-flight measurements constitute major challenges. Not to forget, that Bloch periods typically lie in the femtosecond range and are therefore rather difficult to measure.
The Bloch period has to be much smaller than the average collision times in order for the Bloch oscillations to emerge, which means that the electric field must be strong enough to produce such rapid oscillations. The scattering of electrons from impurities or phonons takes place with a characteristic time of the order of 10^{-13} seconds in a lattice with a representative lattice spacing of a few Ångstroms [16]. The requirements for the field strength can be lowered by increasing the lattice spacing to 10-50 times its original value in an optical lattice. A larger lattice spacing corresponds to a reduced Brillouin zone and therefore smaller Bloch periods while the electric field stays the same.

With respect to numerical errors, the propagator governing our time evolution scheme is prone to gradually lose its unitarity for a large amount of iterative steps in time. For an accurate investigation of long-term behavior a different time evolution procedure will be necessary. A possible approach is provided by the Lindblad master equation formalism that can be used to explicitly construct non-equilibrium steady states [68].
Other extensions could include next-nearest hopping processes and the expansion of the single cluster to encompass larger numbers of lattice sites. Implementing a band Lanczos algorithm, for instance, which is capable of diagonalizing larger single clusters more efficiently than a 'brute force' full diagonalization, could do part of the job of getting closer to an exact description of the system.

Appendix

CPT - Green function formalism

This section primarily follows Refs. [2, 34, 35], see also Ref. [11] for a detailed discussion of Green functions in many-body physics.

Starting from the single-particle Green function

$$G_{\mu,\mathbf{R}_a;\nu,\mathbf{R}_b}(\omega) \;=\; \langle\langle c_{\mu,a} c^{\dagger}_{\nu,b}\rangle\rangle_{\omega} \tag{6.1}$$

we obtain the cluster Green function by decoupling the clusters

$$G^{cl} \;\equiv\; \delta_{a,b} G_{a,\mu,\nu} \tag{6.2}$$

The cluster Green function is diagonal in cluster indices a, b and it is evaluated by use of ED techniques.

The inter-cluster Hamiltonian $\hat{V}$ in (3.4) is treated in strong-coupling perturbation theory. In leading order the obtained lattice Green function has the matrix form

$$\mathbf{G}^{-1} \;=\; \mathbf{G}^{cl\,-1} - \mathbf{V} \tag{6.3}$$

where $\mathbf{V}$ denotes the inter-cluster hopping matrix.

The self-energy Σ is defined by Dyson's equation

$$\mathbf{G}^{-1} \;=\; \mathbf{G}_0^{-1} - \mathbf{\Sigma} \tag{6.4}$$

and the noninteracting Green function has the form

$$\mathbf{G}_0^{-1} \;=\; \omega - \mathbf{T} \;=\; \omega - \mathbf{T}^{cl} - \mathbf{V} \tag{6.5}$$

Here $\mathbf{T}$ stands for the full hopping matrix of the infinite system and $\mathbf{T}^{cl}$ and $\mathbf{V}$ indicate the intra-cluster and inter-cluster hopping matrices respectively.

Rewriting Dyson's equation in terms of $\mathbf{G}^{cl}$ yields

$$\mathbf{G}^{cl\,-1} \;=\; \mathbf{G}_0^{-1\,cl} - \mathbf{\Sigma}^{cl} \tag{6.6}$$

which combined with (6.5) gives

$$\mathbf{G}_0^{-1} \;=\; \mathbf{G}^{cl\,-1} - \mathbf{V} + \mathbf{\Sigma}^{cl} \tag{6.7}$$

Putting this into (6.4) yields the expression

$$\mathbf{G}^{-1} \;=\; \mathbf{G}^{cl\,-1} - \mathbf{V} - \left(\mathbf{\Sigma} - \mathbf{\Sigma}^{cl}\right) \tag{6.8}$$

This relation for the lattice Green function is equivalent to (6.3) if the full self-energy is approximated by the cluster self-energy ($\mathbf{\Sigma} = \mathbf{\Sigma}^{cl}$), resulting in

$$\mathbf{G}^{-1} \;=\; \mathbf{G}_0^{cl} - \mathbf{\Sigma}^{cl} \tag{6.9}$$

Although translational symmetry is broken on the level of the full lattice, invariance is still preservered with regard to the superlattice Γ. $\mathbf{G}^{cl}$ is diagonal in superlattice indices a since it belongs to a particular cluster only. By applying the index transformation $i \to (n, a)$ from lattice indices i to a compound index (n, a) and subsequently performing a partial Fourier transform of the superlattice, which in general reads

$$\mathcal{O}_a \;=\; \frac{1}{\sqrt{N_c}} \sum_{\tilde{\mathbf{k}}} e^{\mathrm{i}\,\tilde{\mathbf{k}}\mathbf{R}_a} \mathcal{O}_{\tilde{\mathbf{k}}} \tag{6.10}$$

we gain

$$\mathbf{G}_{nm}^{-1}(\tilde{\mathbf{k}}, \omega) \;=\; \mathbf{G}_{nm}^{cl\,-1}(\omega) - \mathbf{V}_{nm}(\mathbf{k}) \tag{6.11}$$

This constitutes a mixed representation of the Green function in superlattice wave vectors $\tilde{\mathbf{k}}$ and real space cluster-site indices n, m.

An additional Fourier transform yields the total Green function in $\mathbf{k}$-space, but it would depend on two crystal momenta $\mathbf{k}$ and $\mathbf{k}'$ due to the factorization of the lattice. The off-diagonal terms where $\mathbf{k} \neq \mathbf{k}'$ are neglected by introducing the following periodization prescreption [35] which takes advantage of the fact, that $\mathbf{k}$ and $\mathbf{k}'$ differ only by a wave vector $\mathbf{K}$ of the reciprocal superlattice.

$$\mathbf{G}(\mathbf{k}, \omega) \;=\; \frac{1}{L} \sum_{n,m} e^{\mathrm{i}\,\mathbf{k}(\mathbf{R}_n - \mathbf{R}_m)}\; \mathbf{G}_{nm}(\tilde{\mathbf{k}}, \omega) \tag{6.12}$$

where $\tilde{\mathbf{k}}$ can be replaced by $\mathbf{k}$ since $\tilde{\mathbf{k}} + \mathbf{K}$ yields the same result.

Thus, translational invariance with respect to the total Green function of the full lattice is recovered again.
Note, for further calculations usually the Lehmann representation of Green functions is used.

CPT (in contrast to ED for example) has in principle no limitation on the $\mathbf{k}$-resolution and provides the experimentally relevant spectral function

$$\mathbf{A}(\mathbf{k}, \omega) \;\equiv\; -\frac{1}{\pi} \lim_{\eta \to 0} \mathrm{Im}\, \mathbf{G}(\mathbf{k}, \omega + \mathrm{i}\,\eta) \tag{6.13}$$

for any momentum vector, which is used to compare numerical results with ARPES data. Angle-resolved photoemission spectroscopy is a method of probing the electronic states in momentum space and has become the key experimental technique for comparison with simulated models.

Remark

In the context of C-DMFT the effect of bath sites on the electron Green function is enclosed in the hybridization function [34]

$$\Gamma_{nm}(\omega) \;=\; \sum_{\nu} \frac{\theta_{n\nu}\theta^{*}_{m\nu}}{\omega - \epsilon_{\nu}} \tag{6.14}$$

and the cluster Green function takes on the form

$$\mathbf{G}^{cl\,-1} \;=\; \omega - \mathbf{T} - \mathbf{\Gamma} - \mathbf{\Sigma}^{cl} \tag{6.15}$$

Acknowledgements

First of all I would like to express my thanks to Professor Enrico Arrigoni for all of his help and patience throughout the progression of my work and the formation of this thesis.

Furthermore, I want to thank my friends and colleagues at university, especially Michael Knap, Martin Ganahl and Anna Fulterer for helpful discussions and their kind support, and everybody else with whom I had the chance to get into many interesting and diverting conversations over lunch or a cup of coffee.

Thanks to Andreas Hirczy for almost miraculously tackling any kind of computer- or network-related hardship.

Vicarious for all my friends beyond the corridors of our institute, I would like to thank 차문용 (Cha Moon-Yong) for his reliance and friendship.

Special thanks are devoted to my parents without whom this and so many other things would not have been possible.

Finally, I am grateful to Lisa for inspiring me in many ways.

Bibliography

[1] J. G. Bednorz and K. A. Müller: *Possible high-Tc superconductivity in the Ba-La-Cu-O system.* Z. f. Phy. B Condensed Matter **64**, 189 (1986).

[2] M. Aichhorn: *Ordering phenomena in strongly-correlated systems: cluster perturbation theory approaches.* Ph.D. thesis, Graz University of Technology (2004).

[3] J. A. Slezak, J. Lee, M. Wang, K. McElroy, K. Fujita, B. M. Andersen, P. J. Hirschfeld, H. Eisaki, S. Uchida, and J. C. Davis: *Imaging the impact on cuprate superconductivity of varying the interatomic distances within individual crystal unit cells.* Proceedings of the National Academy of Sciences **105**, 3203 (2008).

[4] J. W. Negele and H. Orland: *Quantum Many-Particle Systems.* Westview Press, Aspen, Colorado, 2nd edition (1998).

[5] H. Tasaki: *The Hubbard model: Introduction and selected rigorous results.* ArXiv:9512169 (1995).

[6] R. Jördens, N. Strohmaier, K. Günter, H. Moritz, and T. Esslinger: *A Mott insulator of fermionic atoms in an optical lattice.* Nature **455**, 204 (2008).

[7] B. Zimmermann, T. Mueller, J. Meineke, T. Esslinger, and H. Moritz: *High-resolution imaging and manipulation of ultracold fermions.* ArXiv:1011.1004 (2010).

[8] C. H. Ahn, J.-M. Triscone, and J. Mannhart: *Electric field effect in correlated oxide systems.* Nature **424**, 1015 (2003).

[9] V. Turkowski and J. K. Freericks: *Nonequilibrium perturbation theory of the spinless Falicov-Kimball model: Second-order truncated expansion in u.* Phys. Rev. B **75**, 125110 (2007).

[10] M. G. Zacher, R. Eder, E. Arrigoni, and W. Hanke: *Evolution of the stripe phase as a function of doping from a theoretical analysis of angle-resolved photoemission data.* Phys. Rev. B **65**, 045109 (2002).

[11] A. L. Fetter and J. D. Walecka: *Quantum Theory of Many-Particle Systems.* Dover Publications, Mineola, New York (2003).

[12] G. D. Mahan: *Many-particle physics.* Plenum Press, New York, 2nd edition (1990).

[13] W. Nolting: *Grundkurs Theoretische Physik 7: Viel-Teilchen-Theorie.* Springer, Berlin Heidelberg, 7th edition (2009).

[14] F. Schwabl: *Quantenmechanik für Fortgeschrittene.* Springer, Berlin Heidelberg, 5th edition (2008).

[15] F. Bloch: Z. Phys. **52**, 555 (1928).

[16] N. W. Ashcroft and N. D. Mermin: *Solid State Physics*. Harcourt College Publishers, Orlando (1976).

[17] J. Hubbard: *Electron correlations in narrow energy bands*. Proc. R. Soc. London A **276**, 238 (1963).

[18] M. C. Gutzwiller: *Effect of correlation on the ferromagnetism of transition metals*. Phys. Rev. Lett. **10**, 159 (1963).

[19] J. Kanamori: *Electron correlation and ferromagnetism of transition metals*. Progress of Theoretical Physics **30**, 275 (1963).

[20] N. M. Peres: *The many-electron problem in novel low-dimensional materials*. Ph.D. thesis, University of Évora (1998).

[21] S. A. Jafari: *Introduction to Hubbard model and exact diagonalization*. ArXiv:0807.4878 (2008).

[22] E. H. Lieb and F. Y. Wu: *The one-dimensional Hubbard model: A reminiscence*. Physica A Statistical Mechanics and its Applications (2003).

[23] C. N. Yang: *Some exact results for the many-body problem in one dimension with repulsive delta-function interaction*. Phys. Rev. Lett. **19**, 1312 (1967).

[24] E. H. Lieb and F. Y. Wu: *Absence of Mott transition in an exact solution of the short-range, one-band model in one dimension*. Phys. Rev. Lett. **20**, 1445 (1968).

[25] J. K. Freericks: *Quenching Bloch oscillations in a strongly correlated material: Nonequilibrium dynamical mean-field theory*. Phys. Rev. B **77**, 075109 (2008).

[26] J. K. Freericks and V. Zlatić: *Exact dynamical mean-field theory of the Falicov-Kimball model*. Rev. Mod. Phys. **75**, 1333 (2003).

[27] J. K. Freericks: *Spinless Falicov-Kimball model (annealed binary alloy) from large to small dimensions*. Phys. Rev. B **47**, 9263 (1993).

[28] E. Dagotto: *Correlated electrons in high-temperature superconductors*. Rev. Mod. Phys. **66**, 763 (1994).

[29] S. R. White: *Density matrix formulation for quantum renormalization groups*. Phys. Rev. Lett. **69**, 2863 (1992).

[30] A. Georges, G. Kotliar, W. Krauth, and M. J. Rozenberg: *Dynamical mean-field theory of strongly correlated fermion systems and the limit of infinite dimensions*. Rev. Mod. Phys. **68**, 13 (1996).

[31] G. Kotliar, S. Y. Savrasov, G. Pálsson, and G. Biroli: *Cellular dynamical mean field approach to strongly correlated systems*. Phys. Rev. Lett. **87**, 186401 (2001).

[32] M. H. Hettler, A. N. Tahvildar-Zadeh, M. Jarrell, T. Pruschke, and H. R. Krishnamurthy: *Nonlocal dynamical correlations of strongly interacting electron systems*. Phys. Rev. B **58**, R7475 (1998).

[33] M. Potthoff: *Self-energy-functional approach: Analytical results and the Mott-Hubbard transition*. European Physical Journal B **36**, 335 (2003).

[34] D. Sénéchal: *An introduction to quantum cluster methods*. ArXiv:0806.2690 (2008).

[35] D. Sénéchal, D. Perez, and M. Pioro-Ladrière: *Spectral weight of the Hubbard model through cluster perturbation theory*. Phys. Rev. Lett. **84**, 522 (2000).

[36] S. Pairault, D. Sénéchal, and A.-M. S. Tremblay: *Strong-coupling expansion for the Hubbard model.* Phys. Rev. Lett. **80**, 5389 (1998).

[37] R. E. Peierls: Z. Phys. **80**, 763 (1933).

[38] V. Turkowski and J. K. Freericks: *Nonlinear response of Bloch electrons in infinite dimensions.* Phys. Rev. B **71**, 085104 (2005).

[39] V. Turkowski and J. K. Freericks: *Nonequilibrium sum rules for the retarded self-energy of strongly correlated electrons.* Phys. Rev. B **77**, 205102 (2008).

[40] H. Bruus and K. Flensberg: *Many-Body Quantum Theory in Condensed Matter Physics.* Oxford University Press, Oxford (2004).

[41] E. Merzbacher: *Quantum Mechanics.* John Wiley & Sons, Inc., Hoboken, NJ, 3rd edition (1998).

[42] C. Lubich: *Integrators for quantum dynamics: A numerical analyst's brief review.* NIC Series **10**, 459 (2002).

[43] D. J. Scalapino, S. R. White, and S. Zhang: *Insulator, metal, or superconductor: The criteria.* Phys. Rev. B **47**, 7995 (1993).

[44] V. V. Deshpande, B. Chandra, R. Caldwell, D. Novikov, J. Hone, and M. Bockrath: *Mott insulating state in ultraclean carbon nanotubes.* Science **323**, 106 (2009).

[45] J. K. Freericks, V. M. Turkowski, and V. Zlatić: *Nonequilibrium dynamical mean-field theory.* Phys. Rev. Lett. **97**, 266408 (2006).

[46] T. Oka and H. Aoki: *Ground-state decay rate for the Zener breakdown in band and Mott insulators.* Phys. Rev. Lett. **95**, 137601 (2005).

[47] F. Heidrich-Meisner, I. González, K. A. Al-Hassanieh, A. E. Feiguin, M. J. Rozenberg, and E. Dagotto: *Nonequilibrium electronic transport in a one-dimensional Mott insulator.* Phys. Rev. B **82**, 205110 (2010).

[48] S. Kirino and K. Ueda: *Nonequilibrium current in the one dimensional Hubbard model at half-filling.* Journal of the Physical Society of Japan **79**, 093710 (2010).

[49] K. M. Shen, F. Ronning, D. H. Lu, F. Baumberger, N. J. C. Ingle, W. S. Lee, W. Meevasana, Y. Kohsaka, M. Azuma, M. Takano, H. Takagi, and Z.-X. Shen: *Nodal quasiparticles and antinodal charge ordering in Ca2-xNaxCuO2Cl2.* Science **307**, 901 (2005).

[50] C. Zener: Proc. R. Soc. London, Ser. A **145**, 523 (1934).

[51] J. Feldmann, K. Leo, J. Shah, D. A. B. Miller, J. E. Cunningham, T. Meier, G. von Plessen, A. Schulze, P. Thomas, and S. Schmitt-Rink: *Optical investigation of Bloch oscillations in a semiconductor superlattice.* Phys. Rev. B **46**, 7252 (1992).

[52] V. G. Lyssenko, G. Valušis, F. Löser, T. Hasche, K. Leo, M. M. Dignam, and K. Köhler: *Direct measurement of the spatial displacement of Bloch-oscillating electrons in semiconductor superlattices.* Phys. Rev. Lett. **79**, 301 (1997).

[53] L. S. Kuzmin and D. B. Haviland: *Observation of the Bloch oscillations in an ultrasmall Josephson junction.* Phys. Rev. Lett. **67**, 2890 (1991).

[54] M. Ben Dahan, E. Peik, J. Reichel, Y. Castin, and C. Salomon: *Bloch oscillations of atoms in an optical potential.* Phys. Rev. Lett. **76**, 4508 (1996).

[55] A. M. Bouchard and M. Luban: *Semiconductor superlattices as terahertz generators.* Phys. Rev. B **47**, 6815 (1993).

[56] W. S. Bakr, J. I. Gillen, A. Peng, S. Fölling, and M. Greiner: *A quantum gas microscope for detecting single atoms in a Hubbard-regime optical lattice.* Nature **462**, 74 (2009).

[57] S. Drenkelforth, G. K. Büning, J. Will, T. Schulte, N. Murray, W. Ertmer, L. Santos, and J. J. Arlt: *Damped Bloch oscillations of Bose-Einstein condensates in disordered potential gradients.* New Journal of Physics **10**, 045027 (2008).

[58] D. Witthaut, F. Trimborn, V. Kegel, and H. J. Korsch: *Quantum dynamics of Bose-Einstein condensates in tilted and driven bichromatic optical lattices.* Phys. Rev. A **83**, 013609 (2011).

[59] A. P. Kampf, M. Sekania, G. I. Japaridze, and P. Brune: *Nature of the insulating phases in the half-filled ionic Hubbard model.* Journal of Physics Condensed Matter **15**, 5895 (2003).

[60] A. P. Kampf: *Magnetic correlations in high temperature superconductors.* Physics Reports **249**, 219 (1994).

[61] A. V. Joura, J. K. Freericks, and T. Pruschke: *Steady-state nonequilibrium density of states of driven strongly correlated lattice models in infinite dimensions.* Phys. Rev. Lett. **101**, 196401 (2008).

[62] B. Moritz, T. P. Devereaux, and J. K. Freericks: *Temporal response of nonequilibrium correlated electrons.* ArXiv:1004.4688 (2010).

[63] F. Claro, J. F. Weisz, and S. Curilef: *Interaction-induced oscillations in correlated electron transport.* Phys. Rev. B **67**, 193101 (2003).

[64] U. Schollwöck: *The density-matrix renormalization group.* Rev. Mod. Phys. **77**, 259 (2005).

[65] S. R. White and A. E. Feiguin: *Real-time evolution using the density matrix renormalization group.* Phys. Rev. Lett. **93**, 076401 (2004).

[66] T. Oka and H. Aoki: *Dielectric breakdown in a Mott insulator: Many-body Schwinger-Landau-Zener mechanism studied with a generalized Bethe ansatz.* Phys. Rev. B **81**, 033103 (2010).

[67] L. Ozyuzer, A. E. Koshelev, C. Kurter, N. Gopalsami, Q. Li, M. Tachiki, K. Kadowaki, T. Yamamoto, H. Minami, H. Yamaguchi, T. Tachiki, K. E. Gray, W.-K. Kwok, and U. Welp: *Emission of coherent thz radiation from superconductors.* Science **318**, 1291 (2007).

[68] T. Prosen: *Third quantization: a general method to solve master equations for quadratic open Fermi systems.* New Journal of Physics **10**, 043026 (2008).

List of abbreviations and symbols

CPT	Cluster Perturbation Theory
VCA	Variational Cluster Approach
DMFT	Dynamical Mean Field Theory
t-DMRG	time dependent Density Matrix Renormalization Group
FK	Falicov-Kimball
ED	Exact Diagonalization
MIT	metal-insulator transition
BZ	Brillouin zone
DOS	density of states
pbc	periodic boundary conditions
hf.	half-filling

t	hopping strength
U	on-site interaction
μ	chemical potential
Δ	staggered on-site potential
E	electric field strength
τ	time
L	sites per cluster
N_c	number of clusters
Λ	total numver of lattice sites
N	total number of itinerant electrons
$\mathbf{k}$	reciprocal lattice wave vector
$\tilde{\mathbf{k}}$	reciprocal superlattice wave vector